Engineering Structures 266 (2022) 114549

Contents lists available at ScienceDirect

Engineering Structures

journal homepage: www.elsevier.com/locate/engstruct

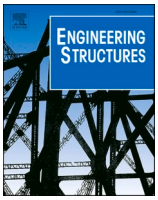

Effect of wave-current interaction on a long fjord-crossing floating pontoon bridge

Jian Dai [a,*], Bjørn Christian Abrahamsen [b], Thomas Viuff [b], Bernt Johan Leira [c]

[a] Department of Civil Engineering and Energy Technology, Oslo Metropolitan University, 0166 Oslo, Norway
[b] SINTEF Ocean, 7052 Trondheim, Norway
[c] Department of Marine Technology, Norwegian University of Science and Technology, 7049 Trondheim, Norway

ARTICLE INFO

Keywords:
Floating bridge
Wave-current interaction
Short-crested
Hydroelastic behaviour

ABSTRACT

Fjord-crossing floating bridges are sophisticated structures subjected to complex environmental loadings including combined action of wave and current. However, the effect of wave-current action is often neglected in a conventional engineering practice. This paper presents a numerical study of the dynamic response of a floating bridge under the combined action of waves and current. The effect of wave-current interaction on the hydrodynamics associated with the bridge pontoons are first evaluated by using a three-dimensional potential flow solver. A model of the entire floating bridge is then established and analysed in the time domain. The accuracy of the model is verified by comparison with available experimental data for a 1 km long curved floating bridge. Parametric studies are subsequently carried out to investigate the effect of wave-current interaction on a 4.6 km long floating bridge model for crossing the Bjørnafjord. Results show that the wave-current interaction has a significant effect on a fjord-crossing floating bridge studied in this paper. Neglection of such an interaction could lead to substantial overestimation or underestimation of the structural responses depending on the environmental headings.

1. Introduction

The Norwegian Public Roads Administration (NPRA) launched a ferry-free coastal highway project along the coastline of Norway. This project aims to reduce the total travel time from Kristiansand in the South to Trondheim in the North (see Fig. 1) by approximately one half using floating bridge technology to connect roads across fjords. Some of the fjords have long crossing spans up to about 5 km. This brings challenges to the design and construction of floating bridge structures. Various design options were proposed and studies were carried out to investigate their performance [1–5].

Floating bridges are often located at exposed areas and consequently they are subjected to complex and combined environmental actions. For example, waves and current are often concurrent in a fjord and they exert loads on the floating parts of a bridge. In the analysis and design of floating bridges, the common practice is to superpose the wave and current loads without considering their interactions [7–9]. However, it is known that waves traveling on current undergo a frequency shift [10,11] and consequently the hydrodynamic properties become different when compared with sea states without current. The modelling of the interaction between waves and current as well as its effect on marine structures have been reported in various studies [12–16]. Most reported works are focused on offshore applications such as drilling and production vessels, piers and wind turbines. Studies investigating the effect of wave and current on floating bridge applications are rather rare. Very recently, Viuff et al. [17] assessed the uncertainty associated with a numerical floating bridge model under wave and current actions via comparison with available model test data. The effect of current speed on wave excitation forces is taken into account. However, the effect on hydrodynamic properties such as added mass and potential damping was ignored.

Furthermore, the water environments inside fjords usually differ significantly from open sea conditions. For example, the wave conditions along the selected bridge crossing site in the Bjørnafjord are relatively calm owing to shielding effects. However, the current speed can exceed 1 m/s [18]. As a result, the effect of current on waves is expected to be more pronounced. Moreover, long floating bridges are slender structures that possess a large number of vibrational modes spanning over a wide frequency range that could be excited by the environmental loads. Consequently, the wave-current interaction may substantially

* Corresponding author.
E-mail address: jiandai@oslomet.no (J. Dai).

https://doi.org/10.1016/j.engstruct.2022.114549
Received 2 November 2021; Received in revised form 10 May 2022; Accepted 11 June 2022
Available online 20 June 2022

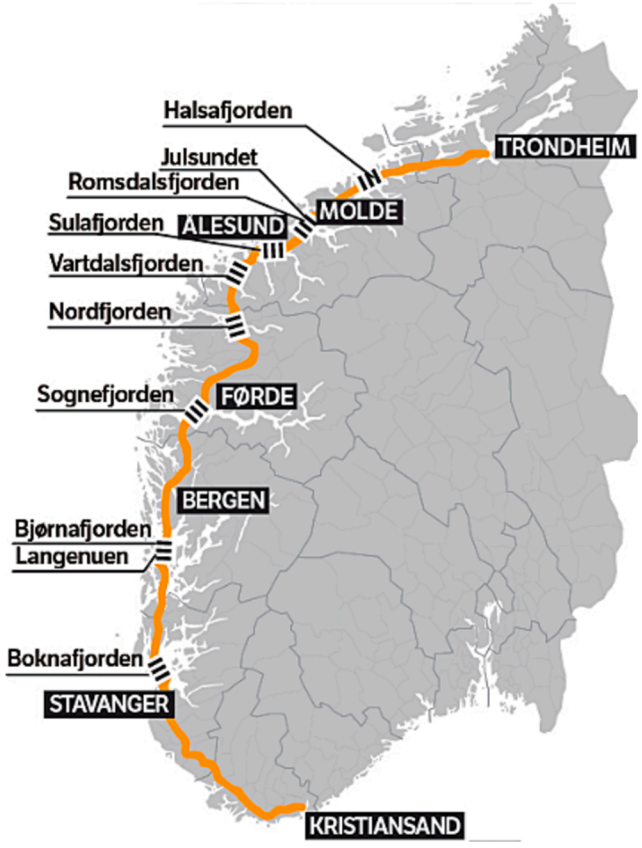

Fig. 1. E39 costal highway route [6].

alter the hydroelastic performance of such slender floating structures. This has important implications on the engineering design practice to ensure safety and cost-effectiveness. Thus, there is an imperative need to understand the dynamic behaviour of floating bridges considering the interaction between waves and current.

In this paper, we present a numerical model for the hydroelastic response analysis of a floating pontoon bridge accounting for the wave-current interaction. The hydrodynamic properties and wave excitation force transfer functions associated with bridge pontoons considering the interaction between waves and current are evaluated in the frequency domain by using the three-dimensional potential flow solver Veres3D. The entire floating bridge model is next constructed by means of the finite element approach in SIMA for the time-domain simulations. The accuracy of the proposed numerical model is examined by comparison with available model test data of a curved floating bridge in the literature. Next, a straight and side-anchored floating bridge model based on the design concept for the Bjørnafjord crossing is put forward to examine the stochastic structural responses. For the purpose of comparison, the bridge responses under three different cases, namely (1) wave load only, (2) wave and current loads without interaction and (3) wave and current loads with wave-current interaction, are investigated. This study attempts to quantify the wave-current interaction effect on the structural responses of a floating bridge and provide useful recommendations and suggestions to researchers and engineers for their study of similar structures.

The remainder of the paper is organised as follows. Section 2 describes the numerical model for the response analysis of a floating bridge considering wave-current interaction. The accuracy of the proposed numerical model is verified in Section 3. Section 4 investigates the effect of wave-current interaction on a 5 km long fjord-crossing floating bridge. Finally, Section 5 concludes the findings of the study.

2. Numerical model and methodology

2.1. Description of floating bridge model

This study investigates the effect of wave-current interaction on a long fjord-crossing floating bridge design. Fig. 2 shows a schematic view of a 4.6 km long bridge model floating over a waterbody with a uniform water depth of 300 m. Note that this bridge model is constructed based on a design concept for crossing the Bjørnafjord [8,9]. The bridge girder is vertically supported by 35 discrete pontoons with an even spacing of 125 m. These pontoons are labelled A1 near the South end of the bridge to A35 near the North end of the bridge. To restrain the lateral motion of the bridge under environmental loads, four identical semi-taut mooring clusters are tethered to the bridge pontoons A6, A14, A22 and A30. Each mooring cluster comprises eight equally pretensioned mooring lines with spiral wire strands sandwiched by studless chain segments. The pretensions for the end clusters (clusters 1 and 4) and the internal clusters (clusters 2 and 3) are 1500 kN and 1630 kN, respective. This ensures that the stiffness of the mooring clusters match that of the design concept [8,9]. The properties of the bridge components are summarized in Table 1. Fixed boundary conditions are applied to the South end of the bridge. At the North end, the restraints on translation along the global x-axis and rotation about the global z-axis are released to allow for possible thermal expansion and planar rotation.

The floating bridge model is constructed by using the finite element method. The bridge girders and columns are modelled using Euler beam elements in view of their slenderness. The mooring lines are modelled using compressionless bar elements. The bridge pontoons are modelled as rigid bodies attached to the lower ends of the bridge columns. The Rayleigh damping model is employed to model the structural damping with a 0.5% damping ratio for the lowest vibration modes for the steel structures [19].

Both mooring lines and bridge pontoons are subjected to hydrodynamic actions induced by waves and water current. For slender mooring lines, the hydrodynamic loads may be evaluated by using the Morison equation [20], which is a semi-empirical equation for the inline force of a slender body in oscillatory flow. The load per unit of the mooring line length can be written as

$$f_m = \rho_w V \ddot{u}_w + \rho_w C_a V\left(\ddot{u}_w - \ddot{u}_m\right) + \frac{1}{2}\rho_w C_d D\left(\dot{u}_w - \dot{u}_m\right)\left|\dot{u}_w - \dot{u}_m\right| \tag{1}$$

where ρ_w is the water density, V is the volume per unit length of the mooring line, D is the diameter of the mooring line, C_a is the added mass coefficient, and C_d is the quadratic drag coefficient. Note that added mass is an analogy to the structural mass and moments of inertia of a body interacting with water. From the physical standpoint, the added mass represents the amount of fluid accelerated or decelerated with the body [21]. The added mass coefficient C_a denotes the ratio of the added mass to the structural mass of the mooring line. Note that the three terms on the right hand side refer to the Froude-Krylov force, the hydrodynamic mass force and the quadratic viscous drag force, respectively [22]. Table 2 lists the coefficients for chain and wire segments according to [23]. $\dot{u}_m$ is the velocity of the mooring line, while $\dot{u}_w$ is the flow speed.

The pontoons can be treated as large volume floating bodies owing to their geometric dimensions. As a result, the potential flow theory [24] is applied to evaluate the wave-induced hydrodynamic actions. The viscous drag and current-induced loads can be accounted for by using the Morison equation considering the quadratic drag term only. The quadratic drag coefficient for bridge pontoons is taken as 0.8 [8,9].

Through global assemblage, the governing equations of motion for the entire floating bridge model can be written as

$$\boldsymbol{M}_B\ddot{\boldsymbol{u}}_B + \boldsymbol{C}_B\dot{\boldsymbol{u}}_B + \int_{-\infty}^{\infty}\boldsymbol{K}_R(t-\tau)\dot{\boldsymbol{u}}_B(\tau)\mathrm{d}\tau + \boldsymbol{K}_B\boldsymbol{u}_B = \boldsymbol{F}_B \tag{2}$$

where $\mathbf{M}_B$ is the global bridge mass matrix that comprises both the

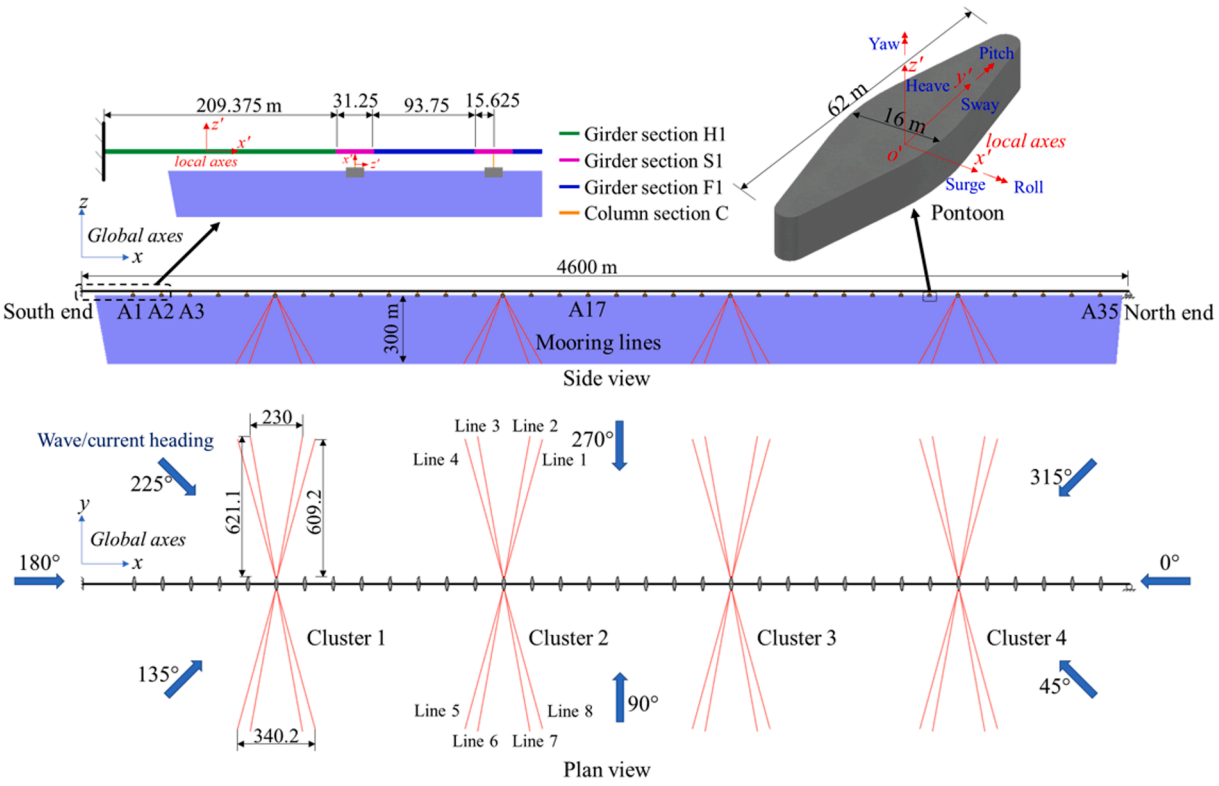

Fig. 2. Floating bridge model.

Table 1
Structural properties of bridge girders, columns, mooring lines and pontoons.

Girder and column	Section			
	H1	S1	F1	C
Mass per unit length	17530 kg/m	19780 kg/m	16040 kg/m	9180 kg/m
Axial stiffness EA_c	2.9×10^8 kN	3.5×10^8 kN	2.5×10^8 kN	3.2×10^8 kN
Flexural rigidity $EI_{y'}$	6.0×10^8 kNm^2	8.5×10^8 kNm^2	6.7×10^8 kNm^2	3.1×10^9 kNm^2
Flexural rigidity $EI_{z'}$	2.3×10^{10} kNm^2	2.4×10^{10} kNm^2	1.9×10^{10} kNm^2	2.0×10^9 kNm^2
Torsional rigidity	4.7×10^8 kNm^2/rad	6.4×10^8 kNm^2/rad	5.4×10^8 kNm^2/rad	2.7×10^9 kNm^2/rad

Mooring line	Segment		
	Top chain	Wire	Bottom chain
Nominal diameter	147 mm	124 mm	147 mm
Length	50 m	600 m	50 m
Mass per unit length	432.2 kg/m	80.3 kg/m	432.2 kg/m
Axial stiffness EA	1.73×10^6 kN	1.42×10^6 kN	1.73×10^6 kN

Pontoon	Type	
	Moored	Unmoored
Weight	1452 tonne	850 tonne
Displacement	5.7×10^3 m^3	3.3×10^3 m^3
Roll inertia	4.2×10^5 tonne m^2	2.2×10^5 tonne m^2
Pitch inertia	6.1×10^4 tonne m^2	2.3×10^4 tonne m^2
Yaw inertia	4.2×10^5 tonne m^2	2.3×10^5 tonne m^2
Heave stiffness	6.7×10^3 kN/m	6.7×10^3 kN/m
Roll stiffness	1.5×10^6 kNm/rad	1.5×10^6 kNm/rad
Pitch stiffness	8.9×10^4 kNm/rad	8.9×10^4 kNm/rad

Table 2
Morison coefficients for mooring lines.

Coefficients	Chain segment	Wire segment
C_a	1.0	1.0
C_d longitudinal	1.5	0.1
C_d transverse	2.4	2.4

structural mass and the hydrodynamic added mass at infinite frequency, $\mathbf{C}_B$ is the global bridge structural damping matrix, $\mathbf{K}_B$ is the global bridge stiffness matrix that contains both the structural stiffness and the hydrostatic restoring stiffness, $\mathbf{F}_B$ is the global load vector that includes the gravitational forces, buoyancy forces, wave excitation forces and viscous drag forces, and $\mathbf{u}_B$ is the global bridge displacement vector. $\mathbf{K}_R$ is the global matrix containing the retardation functions associated with the degrees of freedom of the bridge pontoons. The retardation functions are important for the time-domain sea-keeping analysis [21]. Note that the frequency-dependent added mass and potential damping are included in the calculation of retardation functions that represent the fluid memory effect. The fluid memory effect reflects the physical behaviour that an impulsive displacement experienced by a floating body during a time interval Δt influences the motions of the fluid during this interval as well as during all later time intervals. Similarly, the motions during a certain time interval are influenced by the motions before this interval [25]. Eq. (2) is known as Cummins equation [26] and is widely employed in the time-domain analysis of ships and marine structures considering wave excitations.

In this study, the floating bridge model is constructed in a commercial software package SIMA through the coupled hydro-elastic SIMO-RIFLEX simulations. Note that SIMA [27] is a graphical user interface for SIMO, RIFLEX and coupled SIMO-RIFLEX simulations within the field of marine technology. SIMO [28] is a numerical tool for the simulation of marine operations involving various bodies in the time domain, while RIFLEX [29] is numerical solver for the analysis of slender marine structures. The latter is a nonlinear time domain solver with a finite element formulation that can handle large displacements and rotations. In this study, the pontoon motions are calculated by using SIMO and the slender bridge elements are modelled by using RIFLEX. The geometric nonlinearity of bridge girders and mooring lines are

considered. Also note that the floating bridge model has been validated [4] by comparing the modal properties with available independent studies of the bridge design concept [8,9].

2.2. Modelling wave-current interaction

The bridge pontoons are the main structural components of a floating bridge that are subject to wave and current loads. As stated earlier, potential flow theory often suffices for evaluation of wave-induced actions on a large volume floating body. When the floating body has a complex geometry, researchers and engineers usually resort to powerful numerical approaches. For example, potential flow solvers based on the boundary element method (BEM) such as WAMIT [30] and WADAM [31] which have been extensively validated by both the academia and the industry, are often employed. However, these commonly used solvers usually do not account for the interaction between waves and current.

To include the wave-current interaction, the effect of current speed needs to be accounted for in the formulation of the fluid equations. In this study, Veres3D [32], which is a linear three-dimensional frequency-domain solver based on the boundary element method, is employed. In Veres3D, the theoretical framework adopted by WAMIT and WADAM is extended to account for the wave-current interaction as described by Newman [24]. The linear potential flow theory is based on the assumption that the fluid is incompressible, irrotational and non-viscous. It is employed to evaluate the frequency-dependent hydrodynamic added mass, potential damping and first order wave excitation forces. The non-harmonic and non-linear wave actions such as the quadratic fluid viscous drag will be accounted for by using the Morison equation in this study. Assuming that the current is traveling at a speed U in the negative direction of the global y-axis (see Fig. 3), the velocity potential may be written as a sum of a steady potential and a time harmonic unsteady potential:

$$\Phi = \overline{\phi} - Uy + \varphi e^{i\omega t} \tag{3}$$

where ω is the frequency of the encountered wave, and $\overline{\phi}$ is the disturbance potential of the incident steady flow due to the presence of the floating body. In view of the shape of the pontoon and the current direction, it may be reasonable to simplify the problem by setting $\overline{\phi} = 0$ based on a slender body assumption. The unsteady first order velocity potential φ is given by

$$\varphi = \varphi_0 + \varphi_7 + \sum_{j=1}^{6} \varphi_j \eta_j \tag{4}$$

where φ_0 is the incident wave potential, φ_1 to φ_6 are the radiation wave potential induced by the six degrees of freedom rigid body motion of the pontoon, and φ_7 is the scattering wave potential.

The velocity potential Φ must satisfy the Laplace equation inside the water domain including the boundary conditions. Since the boundary value problem is linear, the different velocity potentials φ_1 to φ_7 can be solved separately. For φ_1 to φ_7 the linearized boundary condition on the mean free surface condition applied in Veres3D is:

$$-\omega^2\varphi + g\varphi_z = 0 \tag{5}$$

where g is the gravitational acceleration. This is the same free surface boundary condition as applied in WAMIT and WADAM.

The body boundary condition enforces that no water can flow into or out from the wet surface of the pontoon. For the radiation potentials φ_j, where $j = 1 - 6$, the body boundary condition applied in Veres3D is written as

$$\frac{\partial \varphi_j}{\partial n} = i\omega n_j + M_j \tag{6}$$

where n is the generalized normal vector on the wet surface of the pontoon. Furthermore, M_1 to M_6 are the terms due to the interaction with the steady flow. In view of the slender body assumption as applied in Veres3D, M_1 to M_4 vanish, leaving $M_5 = n_3 U$ and $M_6 = -n_2 U$.

The body boundary condition for the diffraction potential φ_7 is

$$\frac{\partial \varphi_7}{\partial n} = -\frac{\partial \varphi_0}{\partial n} \tag{7}$$

Then, the wave loads accounting for the wave-current interaction can be computed according to Newman [24]. In comparison, all M_j terms are taken as zero in WAMIT and WADAM. This means that if Veres3D is executed with zero current speed, the mathematical problems solved in Veres3D are identical to those in WAMIT and WADAM. In this study, the frequency-dependent added mass, potential damping and first order excitation forces are evaluated by using Veres3D. With the frequency-dependent hydrodynamic coefficients and force transfer functions available, the equations of motion for the pontoons in the time domain can be written according to Cummins theory [26] as

$$\sum_{k=1}^{6}\left[\left(M_{p,jk} + A_{jk}^{\infty}\right)\ddot{u}_{p,k}(t) + C_{jk}^{b}\dot{u}_{p,k}(t) + \int_{-\infty}^{\infty}\kappa_{jk}(t-\tau)\dot{u}_{p,k}(t)\mathrm{d}\tau + \left(K_{jk}^{h} + K_{jk}^{b}\right)u_{p,k}(t)\right] = F_j^{exc}(t) \tag{8}$$

where j and k refer to the degree of freedom (j, k = 1–6) of a bridge pontoon, and $M_{p,jk}$ is the corresponding structural mass or moment of inertia of a pontoon. Note that the $M_{p,jk} = 0$ when $j \neq k$. A_{jk}^{∞} is the corresponding added mass of a pontoon at infinite frequency, C_{jk}^{b} is the structural damping of the bridge structure, κ_{jk} is the retardation function associated with the jth degree of freedom of the pontoon, K_{jk}^{h} is the hydrostatic restoring stiffness, K_{jk}^{b} is the structural stiffness of the bridge structure, $u_{p,k}$ is the pontoon displacement for the kth degree of freedom, and F_j^{exc} is the wave excitation force corresponding to the jth degree of freedom of the pontoon.

2.3. Environmental conditions

The environmental conditions in a fjord are usually of a complex nature with concurrent wind, waves and current. Moreover, the environmental characteristics exhibit spatial inhomogeneity owing to the large crossing length and complicated topography [33]. As the focus of the present study is on the effect of wave-current interaction on very long fjord-crossing floating bridges, the effect of wind load is not considered. Furthermore, the inhomogeneous environmental effects are out of the scope for the present study and are thus ignored.

There are available current measurement data over a period of 2.5 years at five different locations along the planned bridge crossing. As the field monitoring suffers limitations when measuring the current profile in the water column in the vicinity of the free surface, numerical simulations based on 22 years of hindcast data are employed to compensate for the lack of measurement data [34]. The analysis results show that the current speed exhibits some spatial variations of up to 15% along the crossing. Furthermore, the current speed varies for different directions. The maximum speed at different locations is observed when the current flows out of the fjord (90° as per Fig. 2). For the sake of simplicity, a uniform current speed along the bridge crossing is assumed. Two current

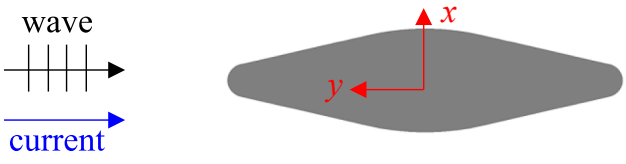

Fig. 3. Wave and current in the longitudinal direction of the pontoon.

directions, namely 90° (out of the fjord) and 270° (into the fjord), are considered. The extreme values of hourly current speed near the free surface are 1 m/s and 1.8 m/s with return periods of 1 and 100 years, respectively. Note that both current speeds apply to the submerged portion of the pontoons. Fig. 4 shows the vertical current speed profiles which are adapted based on the metocean design basis for the Bjørnafjord crossing [18].

According to the design basis for the planned Bjørnafjord's bridge crossing [19], the local wave field is composed of wind-driven waves and swells. However, the swell energy is much lower than the wind wave energy and its effect on the bridge responses is found to be rather small [4,33]. Thus, the swell component is neglected in this study. The wind waves are short-crested and spatially inhomogeneous along the planned bridge crossing [19,33]. The effect of wave inhomogeneity on bridge structural responses and fatigue damage of mooring lines has been investigated earlier [4,35,36]. As a result, this is not considered here since the focus is placed on the interaction between waves and current. According to [19], it is reasonable to model the stochastic wind waves by using the JONSWAP spectrum [37]:

$$S_\zeta(\omega,\theta) = S_\zeta(\omega)D_\zeta(\theta) \tag{9}$$

$$S_\zeta(\omega) = \frac{5}{16}A_\gamma H_s^2\frac{\omega_p^4}{\omega^5}e^{-\frac{5}{4}\left(\frac{\omega}{\omega_p}\right)^{-4}}\gamma^{e^{-\frac{1}{2}\left(\frac{\omega-\omega_p}{\sigma\omega_p}\right)^2}} \tag{10}$$

$$D_\zeta(\theta) = \frac{\Gamma\left(1+\frac{n}{2}\right)}{\sqrt{\pi}\Gamma\left(\frac{1}{2}+\frac{n}{2}\right)}\cos^n\left(\theta-\theta_p\right) \tag{11}$$

where $S_\zeta(\omega,\theta)$ is the directional wave spectrum. By means of separation of variables, it is expressed as a product of the unidirectional wave spectrum $S_\zeta(\omega)$ and the directional spreading function $D_\zeta(\theta)$. $A_\gamma = 1-0.287\ln(\gamma)$, where γ is the non-dimensional peak shape parameter and is set to 2.3 [19]. ω_p is the peak angular frequency and is calculated as $\omega_p = 2\pi/T_p$, where T_p is the wave peak period. σ is the spectrum width parameter which equals 0.07 for $\omega \le \omega_p$ and 0.09 for $\omega > \omega_p$. n is the spreading coefficient and is set to 4 for wind waves in the Bjørnafjord [19]. θ is the incident wave heading, and θ_p is the principal wave direction.

According to the Bjørnafjord bridge design basis [19], design wind wave conditions with large significant wave height H_s and peak period T_p are found within the directional sectors 225–315° and 75–105°. The present study employs the wave conditions with a principal direction that is nearly parallel to the heading of the current. This allows for a clearer investigation of the interaction effect when waves are either propagating with concurrent or adverse directions relative to the water current. The characteristics of the selected design wave conditions are given in Table 3.

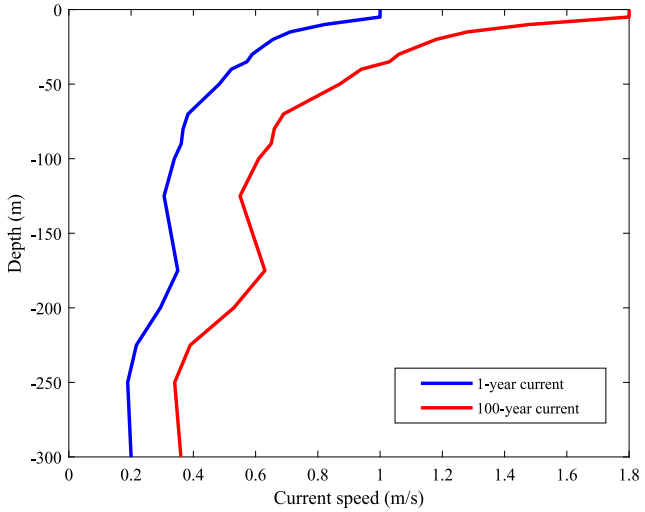

Fig. 4. Vertical current speed profiles.

The irregular wave time history corresponding to a specific wave condition can be obtained from the wave spectrum via Fourier series analysis and expressed as a large number of regular wave components, each with its own wave frequency and amplitude in the frequency domain and a random phase [25]. The wave time history is then used to derive the first order wave excitation forces and the quadratic fluid viscous drag forces for the time domain analysis [4,35].

Table 4 lists the load cases considered in the study. There are two main load cases, namely load case 1 (LC1) and load case 2 (LC2) corresponding to 1-year and 100-year conditions, respectively. Each load case is further composed of three sub-load cases. Sub-load case 1 (LC1.1 and LC2.1) contains wave loads only. Sub-load case 2 (LC1.2 and LC2.2) considers both wave and current loads but neglecting the effect of wave-current interaction. In other words, the wave and current loads are individually calculated and superposed in the simulation. The interaction between waves and current is taken into account for sub-load case 3 (LC1.3 and LC2.3). For the latter two sub-load cases involving current, both scenarios with waves and current travelling in the same direction (LC1.2a, LC1.3a, LC2.2a and LC2.3a) and the opposite directions (LC1.2b, LC1.3b, LC2.2b and LC2.3b) are considered. It should be highlighted that when waves travel with adverse current, small wave components may fail to propagate further in their original heading. The critical wave period can be calculated by ensuring that the wave energy density accounting for the current effect is a real quantity as [10]

$$T_{cr} = \frac{8\pi U\cos\alpha}{g} \tag{12}$$

where T_{cr} is the critical wave period corresponding to the waves that encounter the wave-breaking phenomenon. All smaller waves with a period lower than T_{cr} fail to propagate due to the current. α is the angle between the wave heading and the current direction. Note that the surface current speed is used here in view of the fact that the current speed is constant between the free surface and the submerged portion of the bridge pontoons and that only wave components with small amplitudes and periods fail to propagate under an adverse current. Also Note that the critical wave period is found to be away from the main natural periods of the floating bridge model [4]. Furthermore, wave components with a period smaller than T_{cr} bear less than 10% of the total wave energy. As a result, the affected wave components are not expected to induce large dynamic excitations. Therefore, they are neglected in load cases involving adverse water currents (LC1.2b, LC1.3b, LC2.2b and LC2.3b).

For each load case listed in Table 4, five independent wave realisations are run to reduce the stochastic uncertainties in the results, which is deemed sufficient [4,36]. Each simulation contains an initial 900 s of transient response and subsequent 1-hour steady-state responses. The statistical results presented in the following sections are based on the average of the five independent simulations for each load case.

3. Numerical verification

In an attempt to verify the accuracy of the proposed model for response analysis of a floating bridge accounting for wave-current interaction, the experimental model test of a curved floating bridge conducted by MARINTEK was considered [38]. The floating bridge

Table 3
Selected design wave conditions.

Return period	H_s	T_p	θ_p
1 year	1.3 m	4.6 s	288°
100-year	2.4 m	5.9 s	288°

Table 4
Selected load cases.

Load case	Wave condition	Current condition	Wave-current interaction
LC1.1	1-year wave	No current	–
LC1.2a	1-year wave	1-year current (270°)	No
LC1.2b	1-year wave	1-year current (90°)	No
LC1.3a	1-year wave	1-year current (270°)	Yes
LC1.3b	1-year wave	1-year current (90°)	Yes
LC2.1	100-year wave	No current	–
LC2.2a	100-year wave	100-year current (270°)	No
LC2.2b	100-year wave	100-year current (90°)	No
LC2.3a	100-year wave	100-year current (270°)	Yes
LC2.3b	100-year wave	100-year current (90°)	Yes

tested has a total arch length of 844.8 m and a radius of 1300 m, making a chord length of 830 m in full scale. The bridge is end-anchored with fully restrained boundary conditions for all six degrees of freedom. The girder is elevated 8.8 m above the water surface and vertically supported by eight pontoons. The water depth is set to 100 m and assumed to be constant throughout the entire bridge crossing. Fig. 5 illustrates the experimental model set-up of the floating bridge. The experimental test employed a model scale of 1:40. A detailed description of the floating bridge model was given by Viuff et al. [17]. For ease of reference, the properties of the bridge girder and pontoon and the ballast weights in full scale are given in Tables 5, 6 and 7, respectively.

The same numerical bridge model presented in [17] is employed together with the proposed hydrodynamic model considering wave-current interaction as described in Section 2.2. Note that the modal properties of the floating bridge model were investigated earlier and the accuracy was validated by comparison with available experimental results [17]. As the only difference between the present numerical bridge model and the one in [17] lies in the hydrodynamic modelling of bridge pontoons, the hydrodynamic coefficients and wave excitation forces associated with a bridge pontoon without the effects of current are first evaluated. Fig. 6 compares the hydrodynamic added mass, potential damping and excitation force transfer functions evaluated by the proposed hydrodynamic model and the one reported in [17]. Note that ζ_a in Fig. 6 denotes the wave amplitude, which is half of the incident wave height. For the sake of conciseness, only wave excitation forces related

Table 5
Girder properties [17,38].

Property	Value	Property	Value
Mass per unit length	5.59 tonne/m	Axial stiffness EA_c	5.48×10^9 kN
Flexural rigidity EI_y	1.10×10^9 kNm^2	Flexural rigidity EI_z	2.57×10^9 kNm^2
Torsional rigidity	1.07×10^8 kNm^2/rad		

Table 6
Pontoon properties [17,38].

Property	Value	Property	Value
Mass	1230 tonne	Displacement	2350 tonne
Roll inertia	1.47×10^5 tonne m^2	Pitch inertia	4.42×10^4 tonne m^2
Yaw inertia	2.4×10^5 tonne m^2	Heave stiffness	8.92×10^3 kN/m
Roll stiffness	1.25×10^6 kNm^2/rad	Pitch stiffness	3.21×10^5 kNm^2/rad

Table 7
Ballast weights and elevation from water surface [17,38].

Instrumentation	Weight	Elevation
Instrument	297 tonne	8.8 m
Ballast 1 and 8	462 tonne	1.82 m
Ballast 2 and 7	121 tonne	1.82 m
Ballast 3–6	51.8 tonne	1.82 m
Ballast 9–17	218 tonne	18 m

to a beam sea condition are plotted. As can be seen, both models agree very well with each other despite some minor discrepancies. These discrepancies are believed to arise from different boundary element mesh configurations employed in the two models. Discrepancies are also observed for some properties under long waves with a period above 10 s. These may be explained as being due to the assumption of infinite water depth in the proposed hydrodynamic model. Such an assumption is deemed justifiable in view of the fact that the wave periods inside a fjord are generally small and the water depth is taken as 100 m in the experiment. Note that the actual water depth of a potential fjord crossing can often be larger. Furthermore, the first natural period of the bridge

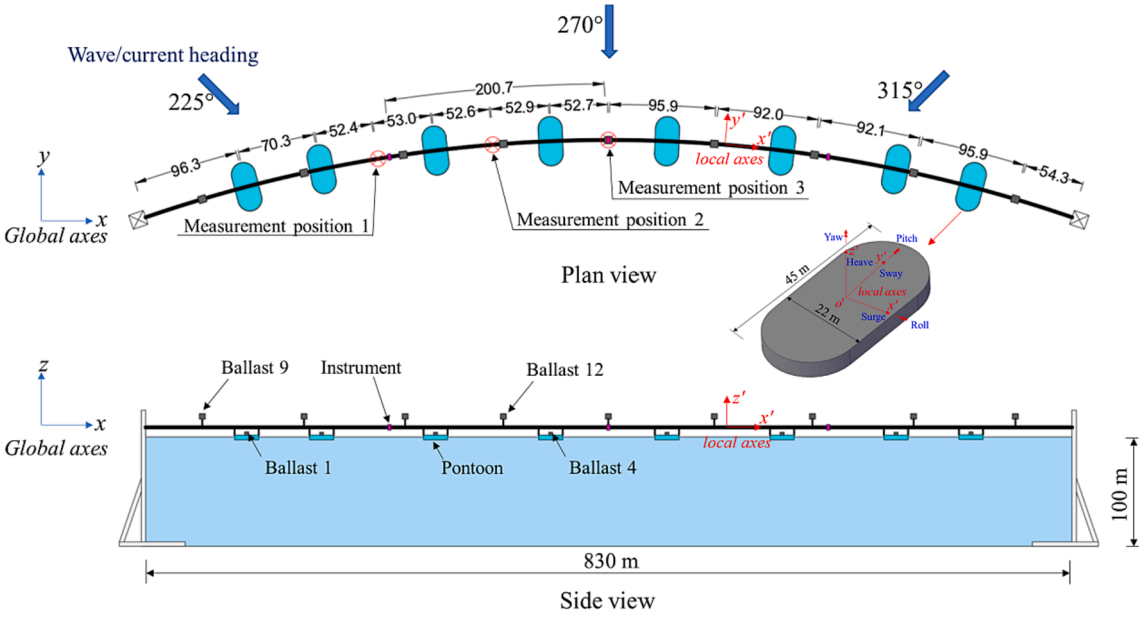

Fig. 5. Schematic view of model test set-up of floating bridge.

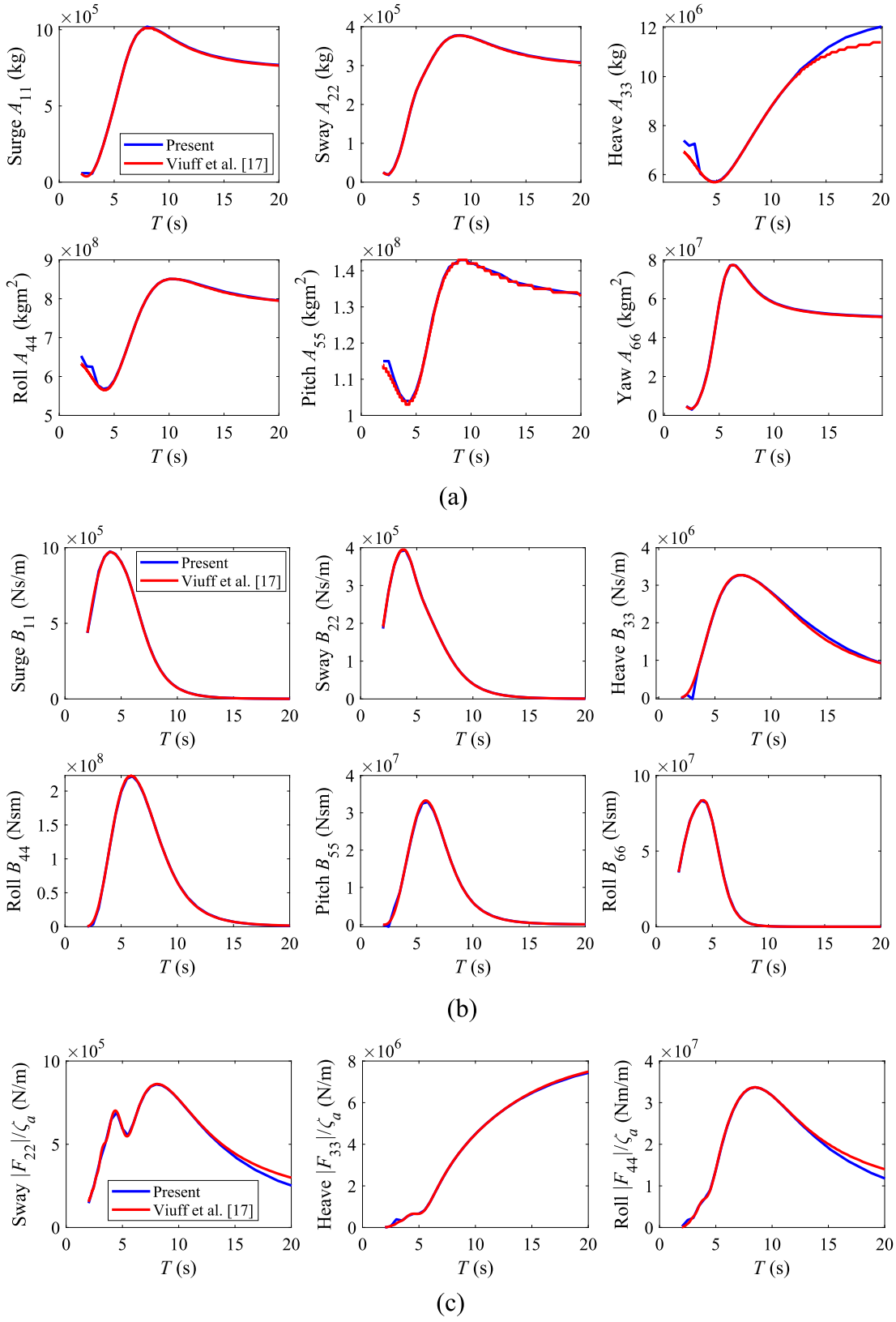

Fig. 6. Hydrodynamic coefficients and excitation forces: (a) added mass, (b) potential damping and (c) first-order wave excitation force transfer function under beam sea condition ($\theta = 270°$).

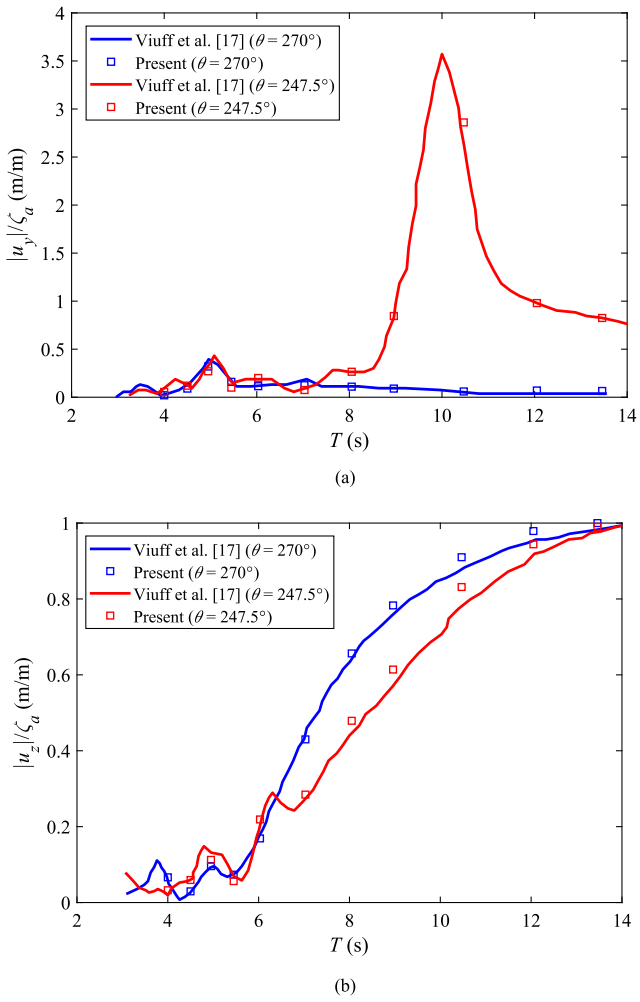

Fig. 7. Motion RAOs of bridge girder at measurement position 1 along (a) y-axis and (b) z-axis.

model in [17] is close to 10 s, which implies that the validation study should not be affected by the difference arising from this assumption.

The motion response of the floating bridge girder under regular wave excitations without current is next examined. Fig. 7 shows the response amplitude operators (RAOs) for the girder motion along the y- and z-axes at measurement position 1 (see Fig. 5). Also plotted in the figure are the results reported by Viuff et al. [17] which have been validated by the experimental data. As can be seen, an excellent match is observed for the transverse motion of the bridge girder under both beam (270°) and oblique (247.5°) waves. The results for the vertical girder motion are also found to agree very well except that small discrepancies are observed for long waves. As already explained, such discrepancies are mainly due to the assumption of infinite water depth in the proposed hydrodynamic model, which is justifiable in view of the actual environmental and topographic conditions. Furthermore, the predicted motion RAOs are slightly larger under long waves, rendering results on the conservative side. Thus, the comparison implies that the accuracy of the proposed hydrodynamic model for wave-induced motions without current is considered satisfactory.

The accuracy of the proposed model for response analysis under irregular wave and current loads is next examined. Table 8 lists four irregular wave test cases conducted in the model test [38]. The first two test cases (test no. 530 and 531) consider irregular waves without current, while the last two cases (test no. 533 and 534) consider concurrent irregular waves and current. Note that all the waves considered here are long-crested and the wave and current headings are identical.

Table 8
Selected load cases.

Test case	Wave condition				Current condition	
	H_s	T_p	θ_p	γ	U	θ
530	1.04 m	4.81 s	270°	3.04	–	–
531	1.44 m	4.93 s	270°	3.33	–	–
533	0.96 m	4.74 s	270°	3.19	0.92 m/s	270°
534	1.64 m	4.87 s	270°	3.21	0.92 m/s	270°

Fig. 8 shows the effect of current on the added mass, potential damping and wave excitation force transfer function associated to a bridge pontoon under beam sea conditions. When there is current propagating in the same direction as the waves, the effect of wave-current interaction is found to affect both the frequency-dependent hydrodynamic coefficients and wave excitation forces, especially for periods below 8 s. More specifically, the added mass and potential damping are generally reduced when waves are travelling with current in the same direction. The magnitudes of the wave excitation force transfer functions tend to be amplified by the current. The frequency range presenting large discrepancies is found to coincide with the wave frequency range of the test cases. Furthermore, the floating bridge possesses many eigenmodes spanning between 3 s and 10 s that can be excited for the tested wave conditions. As a result, the global response of the floating bridge is expected to be substantially influenced by the wave-current interaction.

Fig. 9 shows the standard deviations of the girder motion along the local y- and z-axes at measurement positions 1, 2 and 3. Note that the motion standard deviations are normalized by the significant wave height H_s. For the purpose of comparison, available experimental results [38] and numerical results [17] are also plotted in the same figure. As can be seen, the results generated by the present model agree well with the experimental data for irregular wave load cases (test no. 530 and 531). The difference is generally below 10%, although a larger discrepancy is observed for the vertical motion at measurement position 1. The present model is also found to agree reasonably well with the experimental data for the test cases considering both irregular waves and current. The discrepancies are generally below 15%. Such a discrepancy is often acceptable in engineering practice in view of the uncertainties in both experimental and numerical models. Furthermore, the comparison reveals a substantial improvement in the accuracy when compared with the numerical model that neglects the effect of current on hydrodynamic coefficients [17]. Therefore, it may be concluded that results generated by the proposed model are satisfactory.

4. Response of long fjord-crossing floating bridge

The floating bridge model presented in Section 2 is next employed to investigate the effect of wave-current interaction on structural responses of a 4.6 km long straight and side-anchored floating bridge design concept for the planned crossing of the Bjørnafjord. To illustrate the water current effect on the hydrodynamic properties, Fig. 10 shows the variation of hydrodynamic coefficients and wave excitation forces associated with a typical bridge pontoon due to different current speeds. As can be seen, the hydrodynamic coefficients and wave excitation forces are substantially affected by the current speed in the wave frequency range. In general, the magnitudes of added mass and potential damping decrease for wave periods less than 10 s. Both current speed and direction are found to influence the wave excitation transfer functions. For the same wave frequency range, the magnitudes of wave excitation transfer functions are increased for cases where the waves and current are acting in the same direction, whereas a reduction is observed for cases involving waves and current travelling in the opposite directions. It is thus expected that the presence of current has an important effect on the global responses of the floating bridge.

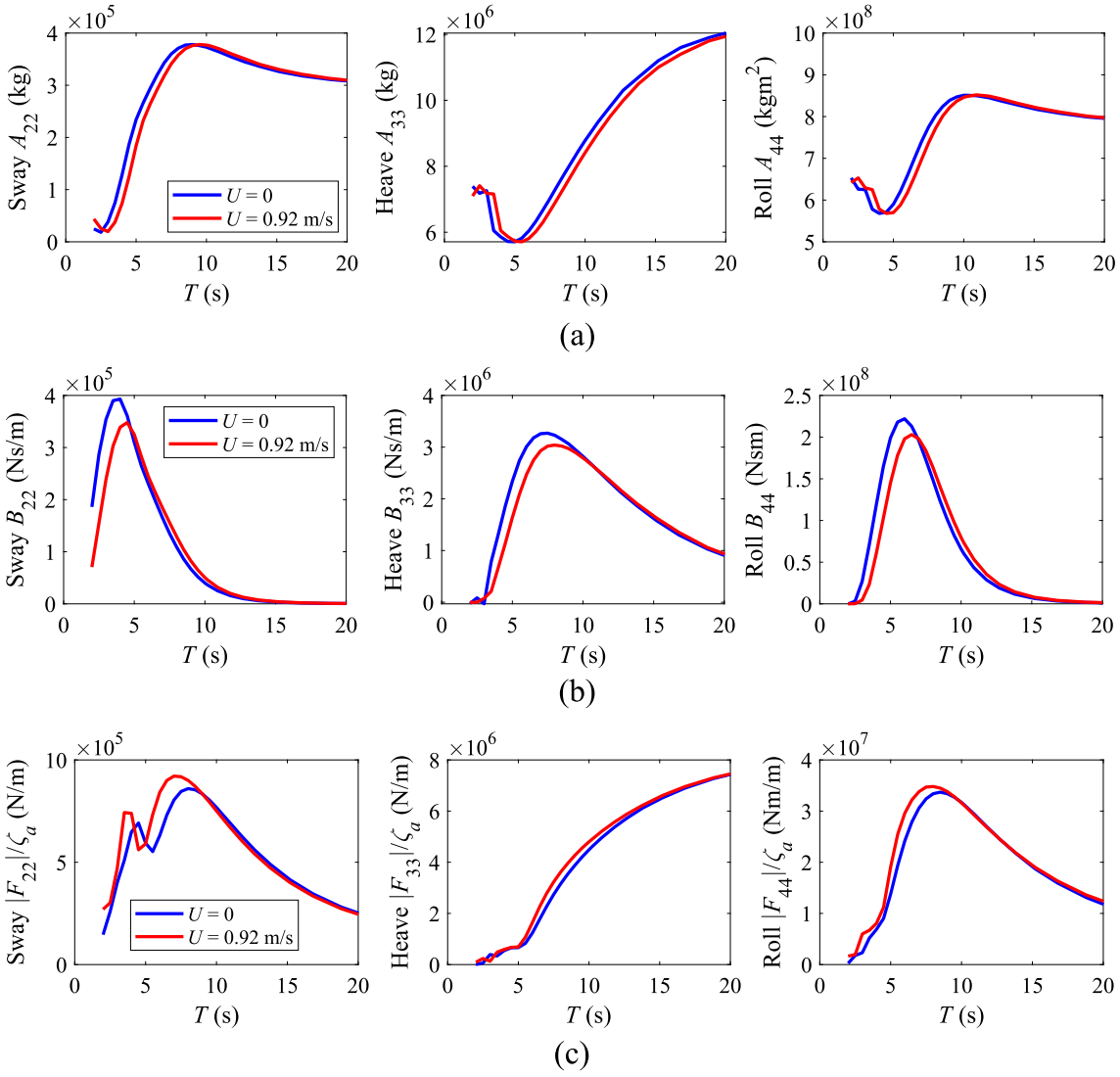

Fig. 8. Effect of current on hydrodynamic coefficients and excitation forces: (a) added mass, (b) potential damping and (c) first-order wave excitation force transfer function under beam sea condition ($\theta = 270°$).

4.1. 1-year load effects (LC1)

The dynamic response of the floating bridge when subjected to 1-year load cases is first investigated. The focus is placed on the bridge girder as it is the key structural component of the floating bridge system. Note that the statistical responses including the maximum, mean and standard deviation values are presented and discussed. The maximum values are directly related to the design practice of a floating bridge. The mean values and standard deviations are usually not directly applied in the design practice, but they are important statistical parameters which provide useful insight and guidance for the design. For example, the mean values refer to the static or quasi-static responses of the structural components and they can be used e.g., precambering and prestressing of the key structural members during the construction phase. The response standard deviations are an important indicator of the quality of the stochastic results and thus the confidence in using the data in the design procedure. Furthermore, they provide useful insight for the fatigue analysis and design of the bridge components [36]. Fig. 11 shows the statistical results for the weak axis bending moment M_y along the bridge girder. As can be seen, the maximum and mean values are virtually unaffected by the presence of current and its effect on the waves. This is due to the fact that the weak axis bending moment is governed by the self-weight of the bridge. For the standard deviations, the presence of current and neglection of the interaction with waves (LC1.2a and LC1.2b) also does not induce a noticeable difference from the wave only load case (LC1.1). However, discrepancies are observed when the interaction between waves and current is considered. The standard deviations in M_y are substantially amplified when both the waves and current propagate in the same direction (see LC1.3a). The amplification is between 30% and 52%. This is expected in view of the amplified wave excitation forces in the wave frequency range as compared to LC1.1. When the current is travelling in the opposite direction relative to the waves, however, LC1.3b results in slightly reduced standard deviations for M_y as compared to LC1.1. The average reduction is around 7% along the girder. The statistical results for the M_y responses imply that although the wave-current interaction may not affect the strength design of the bridge girder pertaining to the weak axis bending, it may lead to an underestimated fatigue damage if such an effect is ignored.

Fig. 12 shows the statistical results for the strong axis bending moment M_z along the bridge girder. In contrast to the weak axis bending moment, the presence of current affects both the maximum, mean and standard deviation values of M_z. When the interaction between waves and current is neglected, the current and its flow direction have a small effect on the maximum M_z. The standard deviations are even found to be on average 6% smaller than for LC1 due to the damping effect arising from the quadratic viscous drag. However, when the wave-current

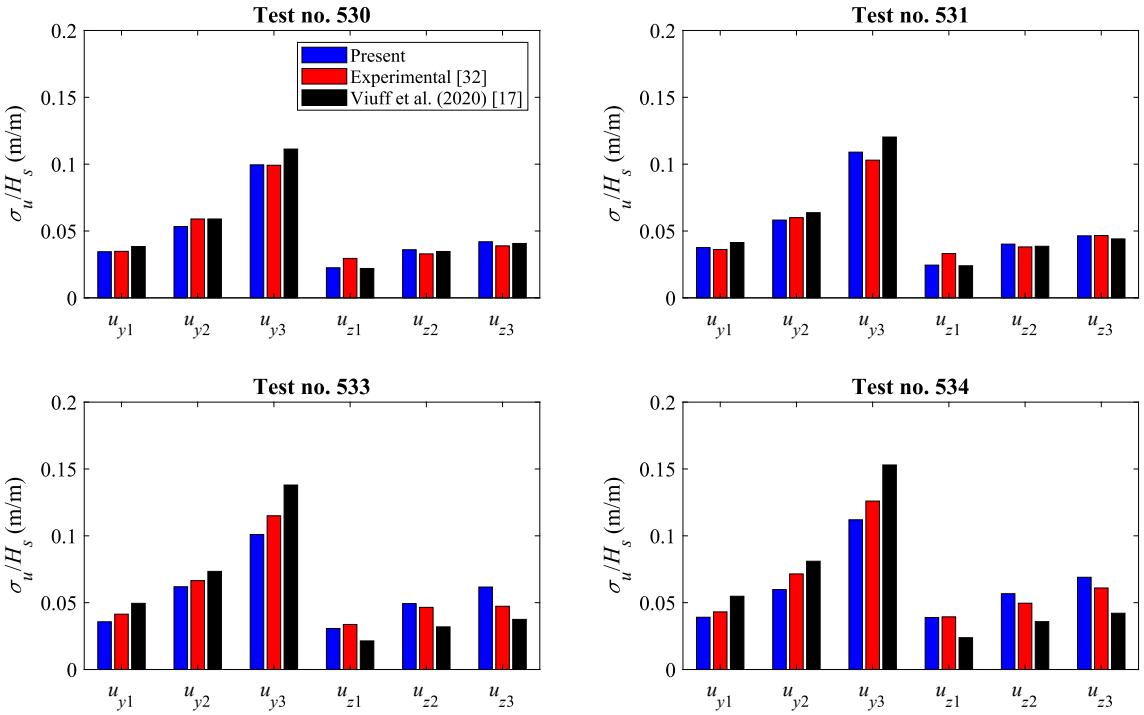

Fig. 9. Standard deviations of bridge girder motion for different test cases.

interaction is taken into account, both the current speed and flow direction are found to strongly affect the maximum values and standard deviations of M_z responses. More specifically, they are substantially amplified when the current and waves are travelling in the same direction, whereas a reduction in the responses is found when their directions are opposing each other. The amplification in the standard deviation is up to 36% and the reduction is up to 33%. Due to the fact that the mean values are governed by the viscous drag due to current and that the slowly varying second order wave excitation forces are neglected in this study, the mean values of M_z are not affected by the wave-current interaction effect.

Figs. 13 and 14 show the statistical results of the axial force F_x and torsional moment T along the bridge girder, respectively. Similar to the strong axis bending moment responses, both the maximum values and standard deviations are strongly affected by the presence of current when considering the wave-current interaction effect. In general, a significant increase of the responses is observed when the waves and current are propagating in the same direction, whereas a reduction in the response is found when they are travelling in the opposite directions. When the wave-current interaction effect is neglected, the maximum values and standard deviations of both F_x and T responses are slightly smaller than for LC1 and they are virtually unaffected by the current direction except for the maximum responses of T in which the current direction has some effects in the vicinity of the mooring clusters.

As 1-year environmental conditions are often employed for assessing the serviceability of the bridge, motion responses of the girder are next investigated. According to Lwin [13], the wave-induced girder motions should not exceed 0.3 m along both transverse and vertical directions under operational (1-year storm) conditions. Meanwhile, the wave-induced girder accelerations should not exceed 0.5 m/s^2 in both directions. Note that the objective of this study is to quantify the effect of wave-current interaction on bridge girder responses with selected wave and current conditions. The detailed design checks need to consider all relevant environmental conditions including the wind action, traffic conditions and the combinations of different actions, which is out of the scope of this study. Figs. 15 and 16 show the displacement and acceleration statistics of the bridge girder along the y-axis, respectively. As can be seen, the presence of water current without considering the wave-current interaction leads to much amplified maximum responses of the transverse displacement. When the interaction between waves and current is taken into account, the current direction has some effects on the maximum displacements of the bridge girder and both cases lead to much amplified responses when compared with LC1.1. Such an effect is found to be much smaller when compared with the maximum acceleration responses. This is expected owing to the fact that the current has little effect on the mean accelerations of the bridge girder. Both the wave-induced transverse displacements of the bridge girder (maximum displacements subtracting the mean values due to current effect) and accelerations are found to be within the suggested operational design limits. The effects of current speed and interaction between waves and current on the standard deviations of motion responses are found to be very similar to those for the M_z responses.

Figs. 17 and 18 show the statistical results of the displacement and acceleration, respectively, of the bridge girder along the z-axis. Similar to M_y responses, the current speed and direction have a rather small effect on the maximum and mean values of the vertical displacement of the bridge girder. Again, this is due to the fact that they are primarily governed by the self-weight of the girder. When it comes to the girder accelerations where the effect of the static components is not included, the presence of current when neglecting the wave-current interaction (LC1.2a and LC1.2b) has virtually no effect on the maximum acceleration responses when compared to LC1.1, except for a slight reduction arising from the viscous drag effect. When the coupling between waves and current is taken into account, the maximum girder accelerations are much amplified when the waves are travelling in the same direction as the current (LC1.3a). The maximum values are found to be around 0.46 m/s^2, which is very close to the suggested operational limit of 0.5 m/s^2 under serviceability limit state [39,40]. However, if the wave-current interaction effect is neglected as in the conventional analysis and design of a floating bridge or similar marine structures, the motion responses may be substantially underestimated. This could potentially lead to unsafe designs jeopardizing the travel safety of road users. On the other hand, when the waves and current are acting in the opposite directions (LC1.3b), a slight reduction is generally observed. Similar

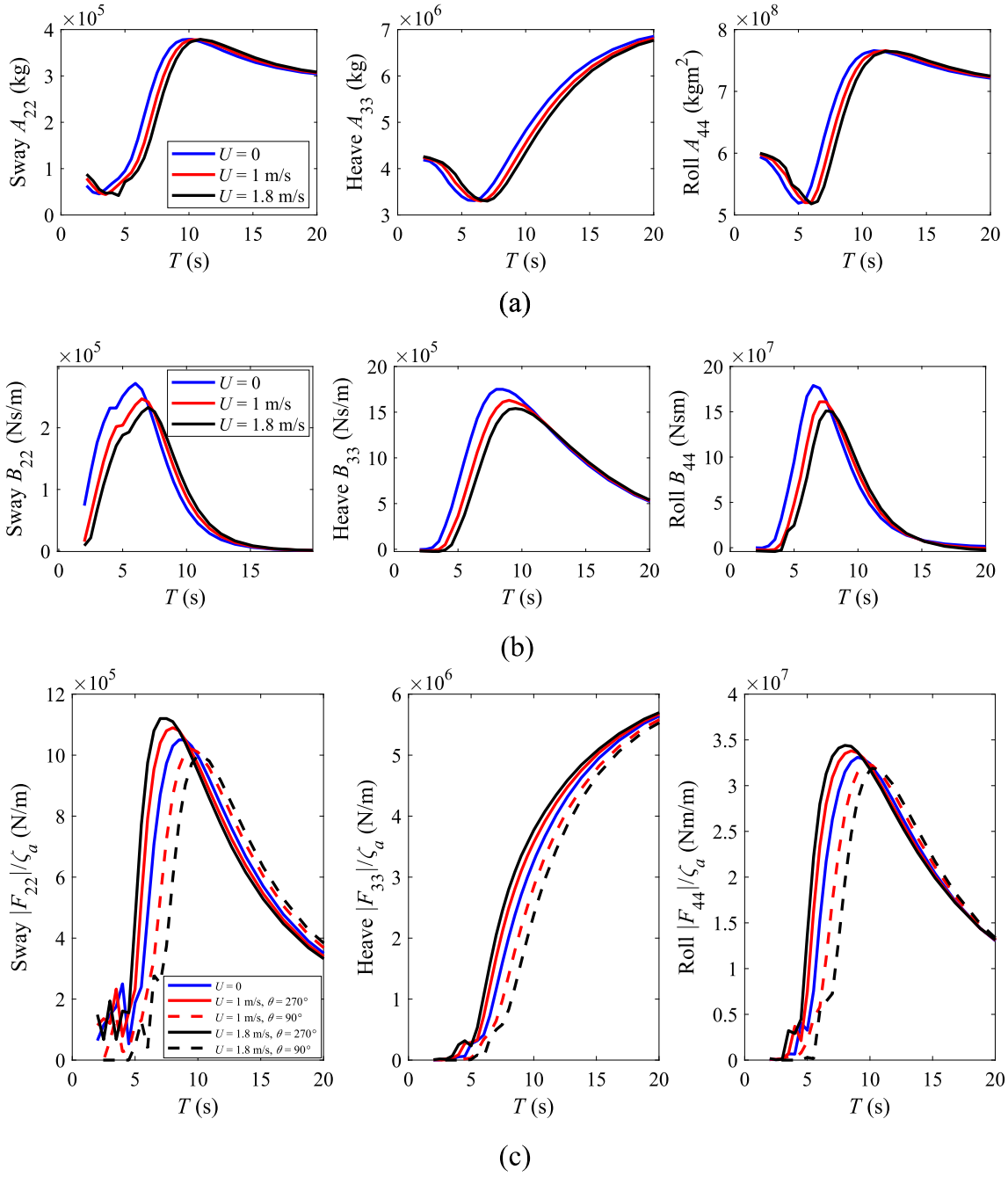

Fig. 10. Effect of current on hydrodynamic coefficients and excitation force: (a) added mass, (b) potential damping and (c) first-order wave excitation force transfer function for beam sea conditions ($\theta = 270°$).

observations are found for the standard deviations of both vertical displacements and accelerations.

4.2. 100-year load effects (LC2)

The dynamic response of the floating bridge for the 100-year load cases is next investigated. The 100-year wave and current conditions are much harsher than the 1-year conditions (see Section 2.3) and thus they are often used in the ultimate limit state analysis and design. Fig. 19 shows the statistical values of the bending moment along the bridge girder about the global y-axis. Similar to the 1-year M_y responses, the presence of current without considering the wave-current interaction has virtually no effect on the 100-year M_y responses. When the effect of current on the waves is taken into account, the standard deviations in M_y experiences a 56%-122% increase when the waves and current are propagating in the same direction. The amplification is virtually doubled as compared to the 1-year load cases as a result of a much increased current speed associated with the 100-year load case LC2.3a. This has also led to a noticeable increase in the maximum M_y responses when compared with other load cases despite the large contribution from the girder's self-weight. When the waves are travelling against the current (LC2.3b), an average reduction of 10% in the standard deviations is observed as compared to LC2.1.

The statistical results of the strong axis bending moment M_z along the bridge girder induced by various load cases shown in Fig. 20 share similar observations with the 1-year results. Owing to the much higher current speed in a 100-year condition, LC2.3a induces an average increase of 50% in the standard deviations when compared with LC2.1.

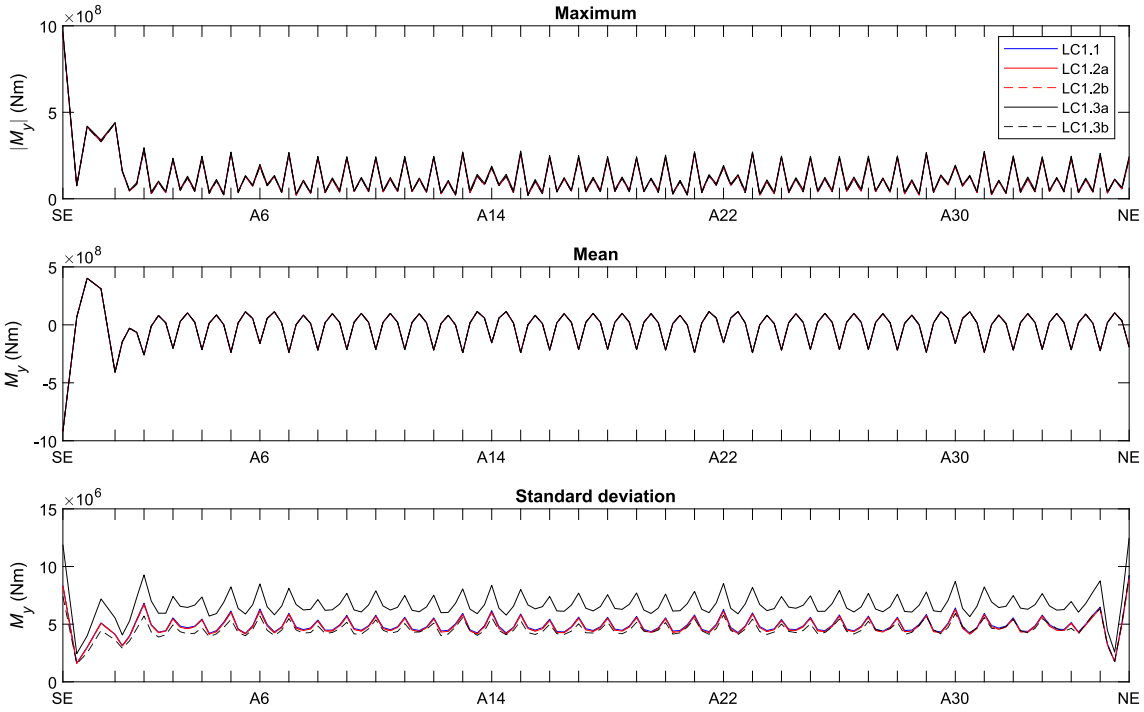

Fig. 11. Statistical values of weak axis bending moment for 1-year load cases.

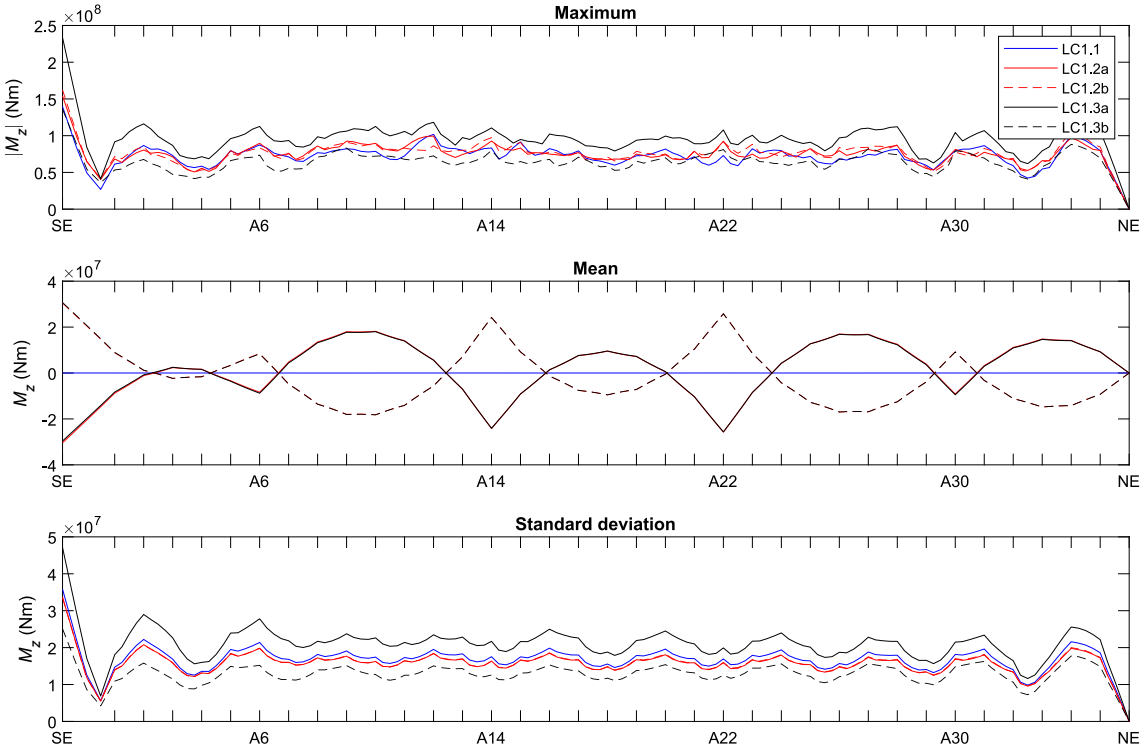

Fig. 12. Statistical values of strong axis bending moment for 1-year load cases.

The maximum increase of 73% is observed near the South end while the amplification is gradually reduced as it moves towards the North end. When the wave heading is opposing the current direction, LC2.3b is found to result in reduction of up to 53%, which is also much larger than for the 1-year load cases.

Figs. 21 and 22 show the statistical results for the axial force and torsional moment, respectively, along the bridge girder corresponding to the 100-year load cases. As compared to the 1-year responses, the larger current speed amplifies the wave-current interaction effects on the bridge responses. For example, LC2.3a results in up to 67% increase in both the maximum axial forces and the standard deviations when compared with LC2.1, while for the 1-year load cases such an increase is less than 30%. Furthermore, the larger current speed also has an effect on the torsional responses even when the wave-current interaction is

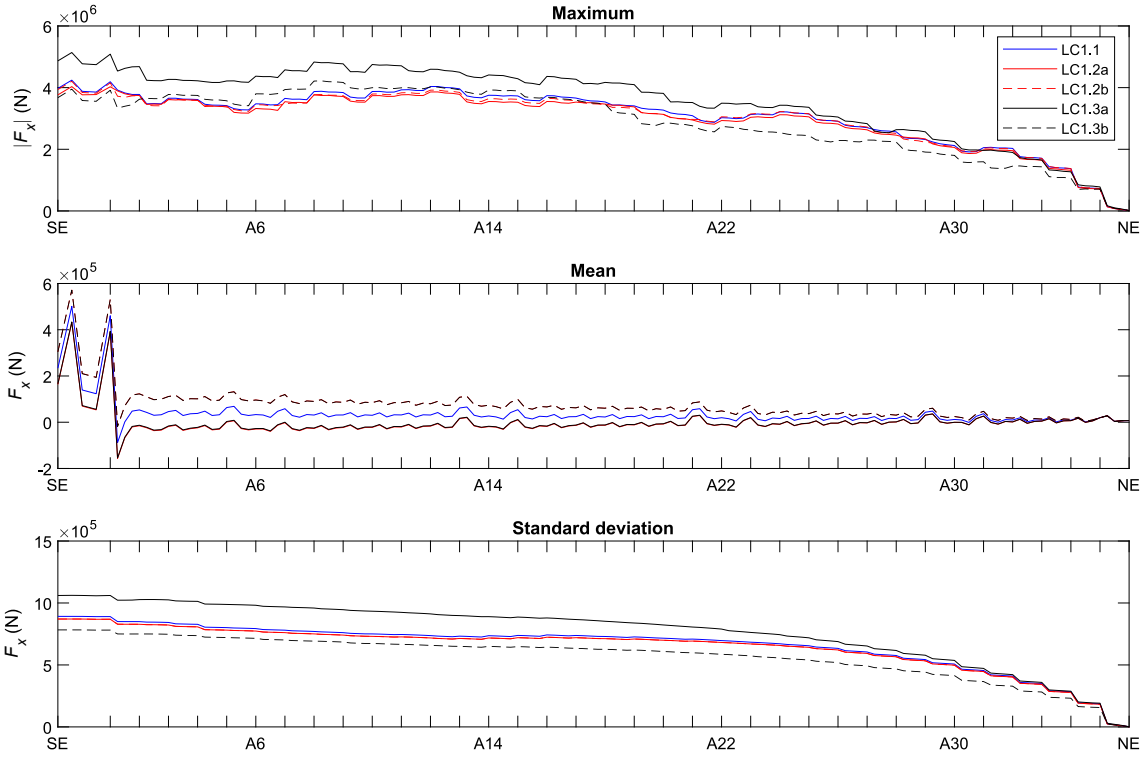

Fig. 13. Statistical values of axial force for 1-year load cases.

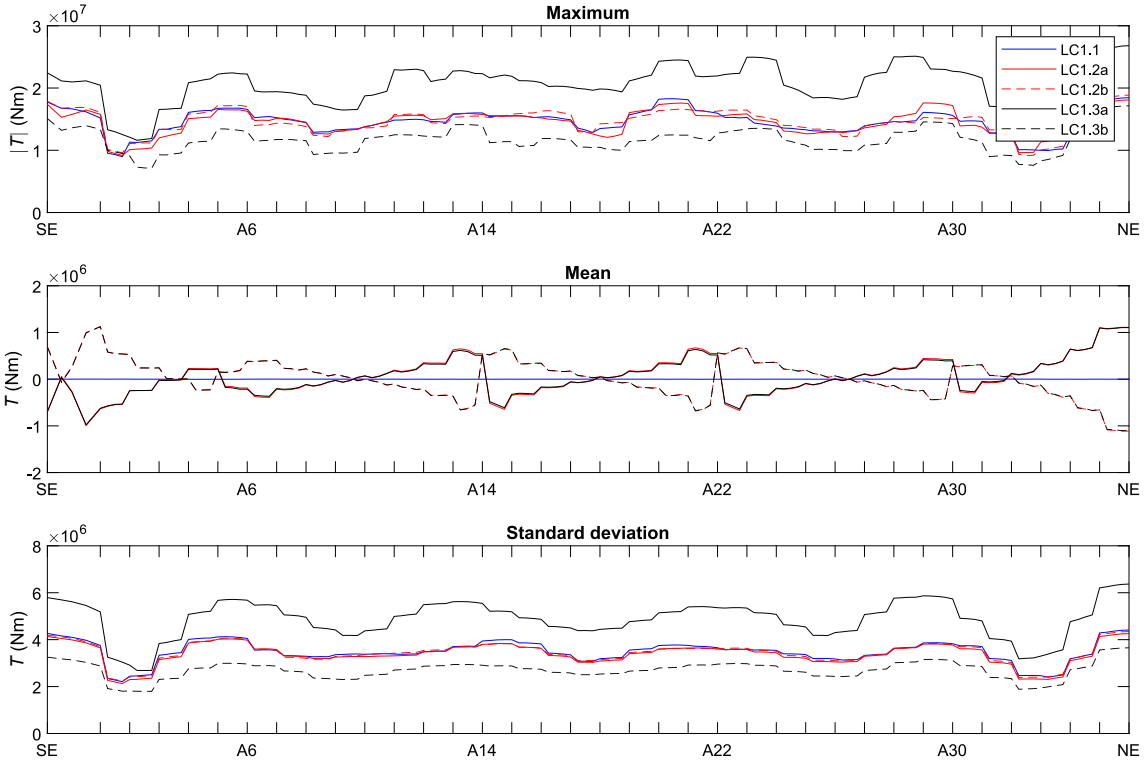

Fig. 14. Statistical values of torsion for 1-year load cases.

neglected. LC2.2b is found to induce slightly larger torsional moments than LC2.1 and LC2.2a in terms of maximum responses and standard deviations.

5. Conclusions

This paper is concerned with a numerical study of the global structural responses of a 5 km long floating bridge under the combined action of waves and current considering the wave-current interaction. The

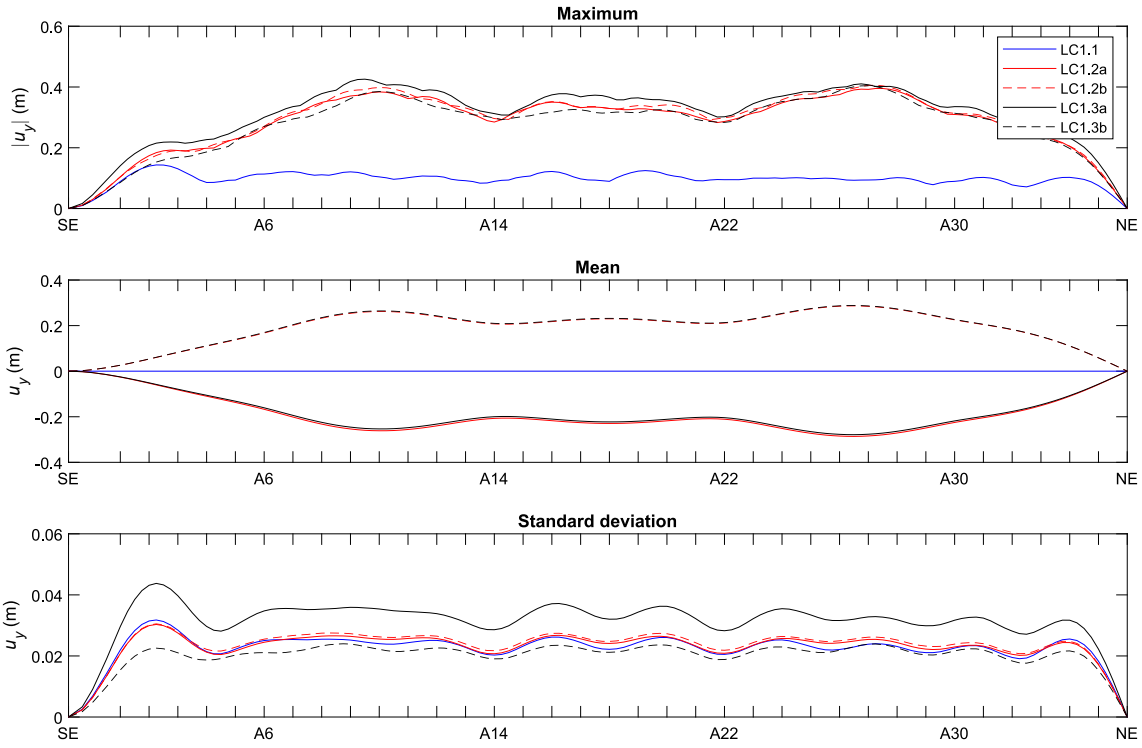

Fig. 15. Statistical values of transverse displacement for 1-year load cases.

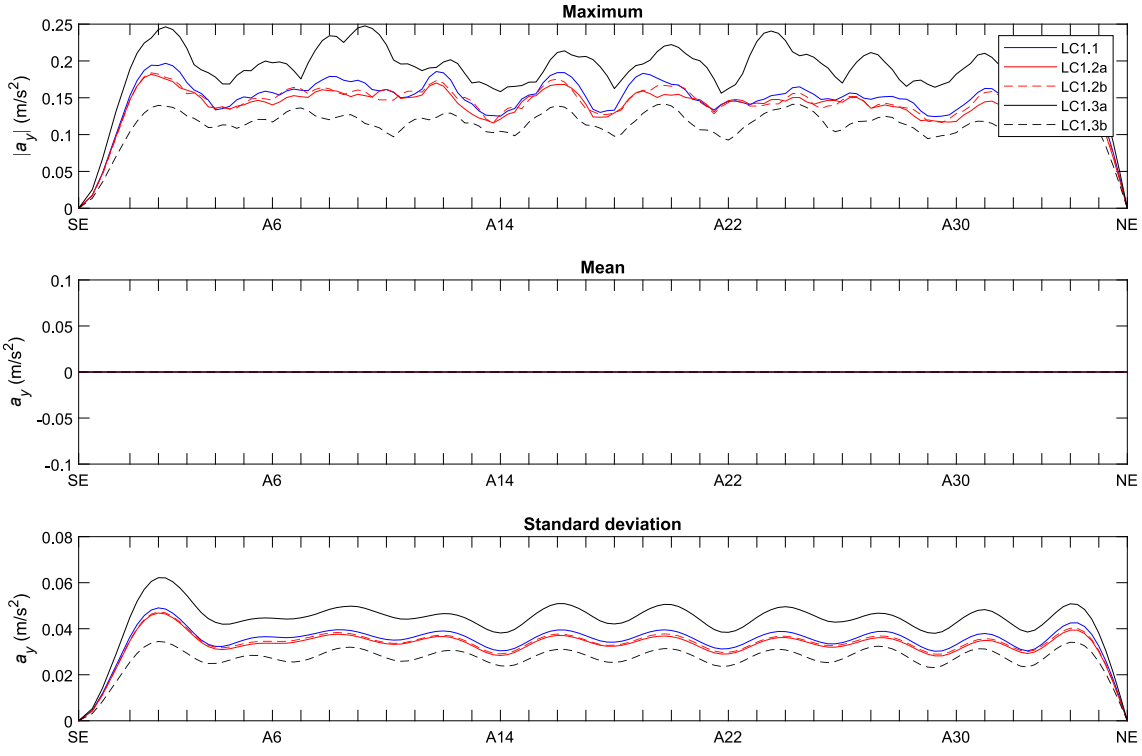

Fig. 16. Statistical values of transverse acceleration for 1-year load cases.

accuracy of the proposed computational model is validated by comparison with available experimental data and numerical results for a curved floating bridge which is described in the literature. Next, a straight and side-anchored floating bridge model based on the Phase 3 design concept for the Bjørnafjord crossing is put forward to examine the stochastic structural responses. For the purpose of comparison, the bridge responses under different cases considering various combinations of wave and current, their interaction effects and two different return periods are investigated. Analysis results show that when waves travel with current in the same direction, the wave-current interaction effect can significantly amplify the bridge responses. The level of amplification increases with the speed of the current. Under 1-year load cases, the

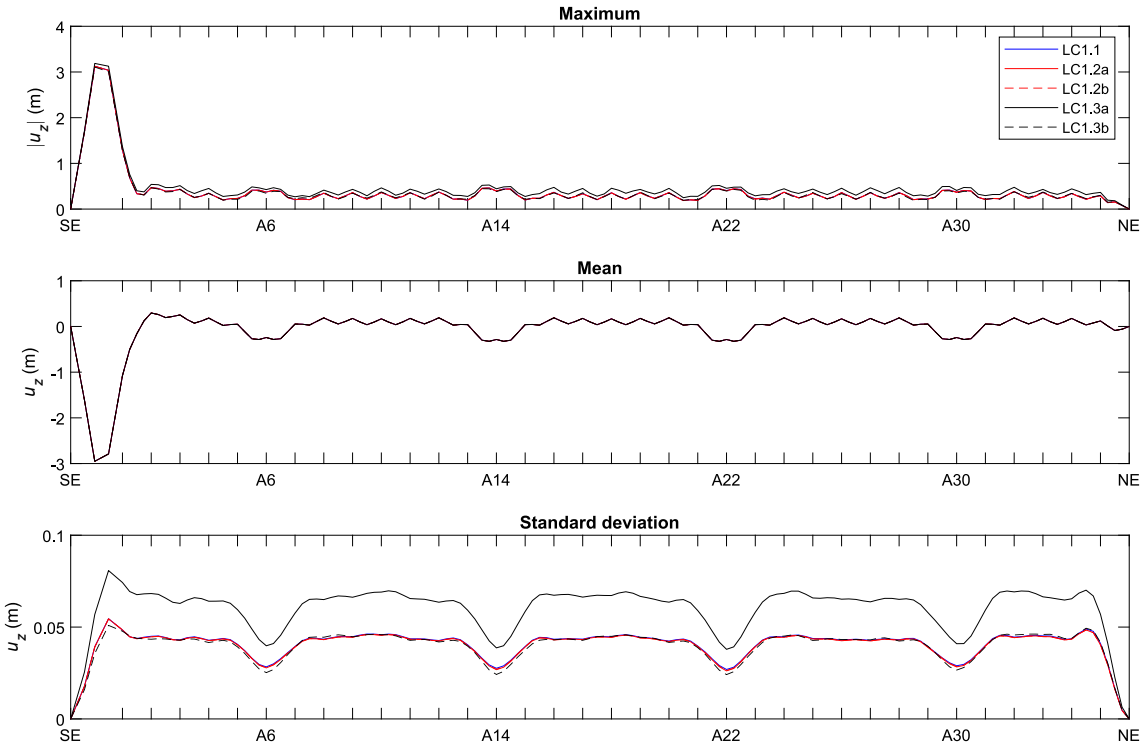

Fig. 17. Statistical values of vertical displacement for 1-year load cases.

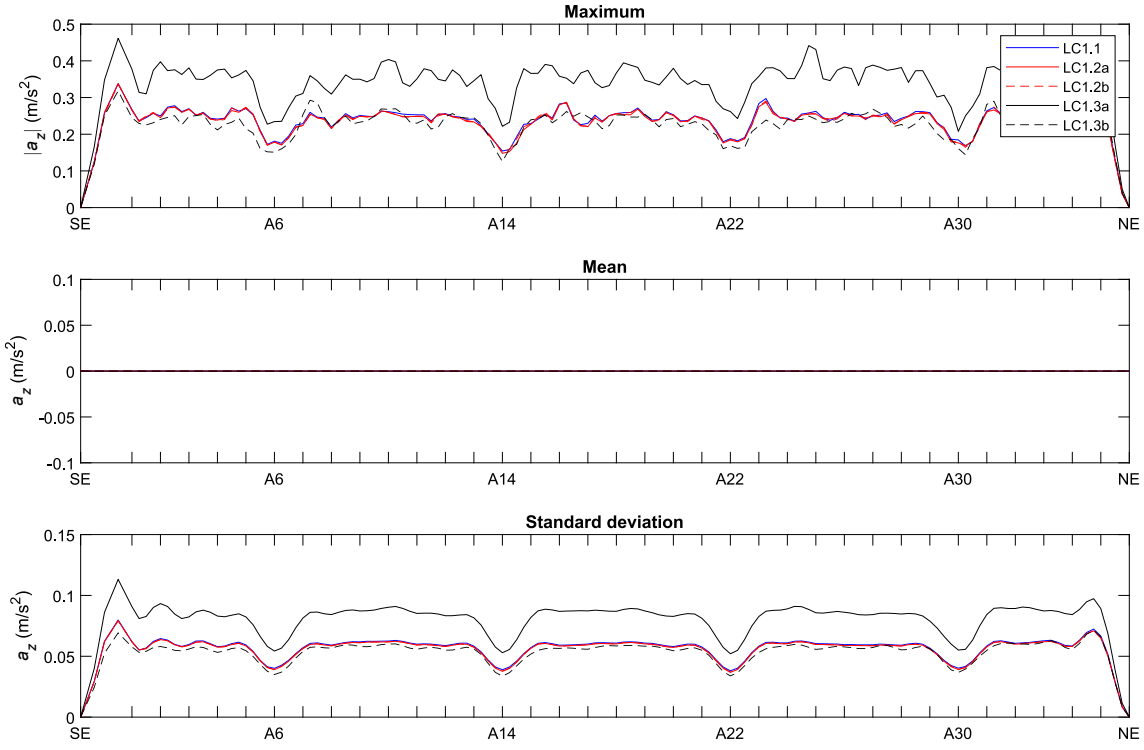

Fig. 18. Statistical values of vertical acceleration for 1-year load cases.

amplifications in the standard deviations, which reflect the dynamic components of the results, in the weak axis bending M_y, strong axis bending M_z and axial force F_x are found to be up to 52%, 36% and 30%, respectively. Under 100-year load cases, such amplifications in M_y and F_x are up to 122% and 67%, which are more than doubled as compared to those under 1-year load cases, while M_z experiences a 50% increase generally. However, when the interaction effect is ignored, the common design practice of superposing wave and current loads may lead to slightly lower bridge responses than the case neglecting current due to the viscous drag effect. Accordingly, a significant underestimation could arise if the wave-current interaction effect is ignored.

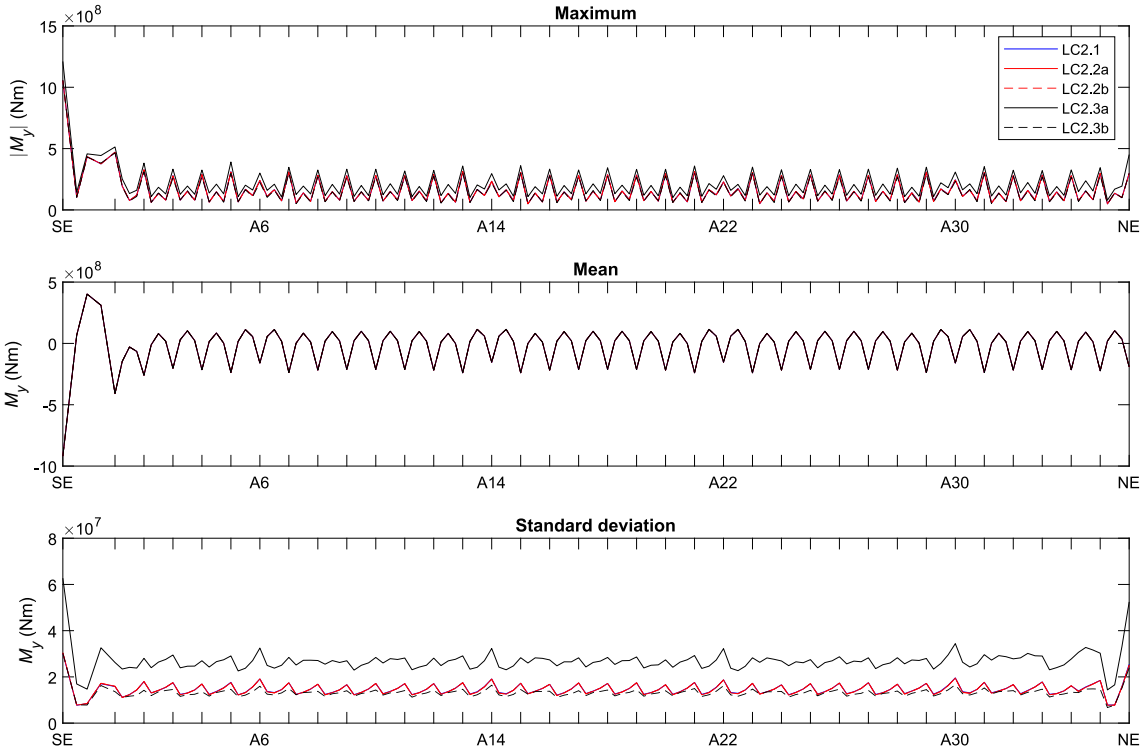

Fig. 19. Statistical values of weak axis bending moment for 100-year load cases.

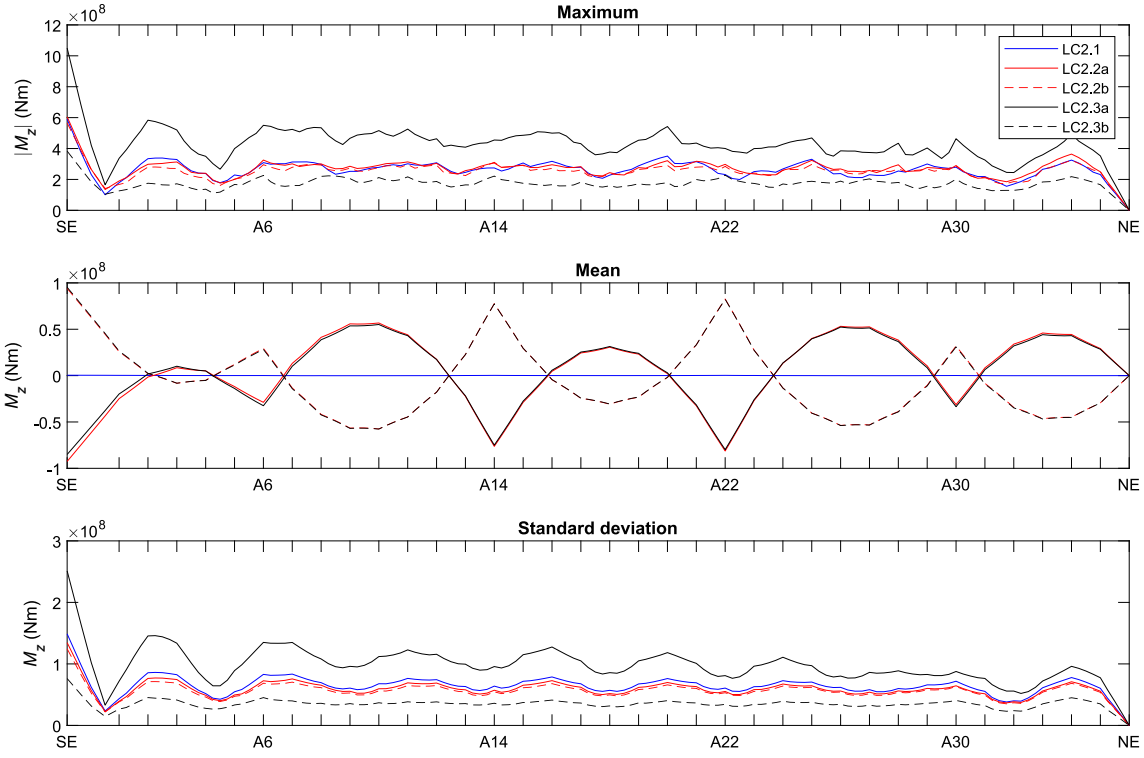

Fig. 20. Statistical values of strong axis bending moment for 100-year load cases.

CRediT authorship contribution statement

Jian Dai: Conceptualization, Methodology, Formal analysis, Validation, Writing – original draft, Visualization. **Bjørn Christian Abrahamsen:** Conceptualization, Methodology, Software, Writing – review & editing. **Thomas Viuff:** Methodology, Resources, Writing – review & editing. **Bernt Johan Leira:** Conceptualization, Writing – review & editing, Supervision.

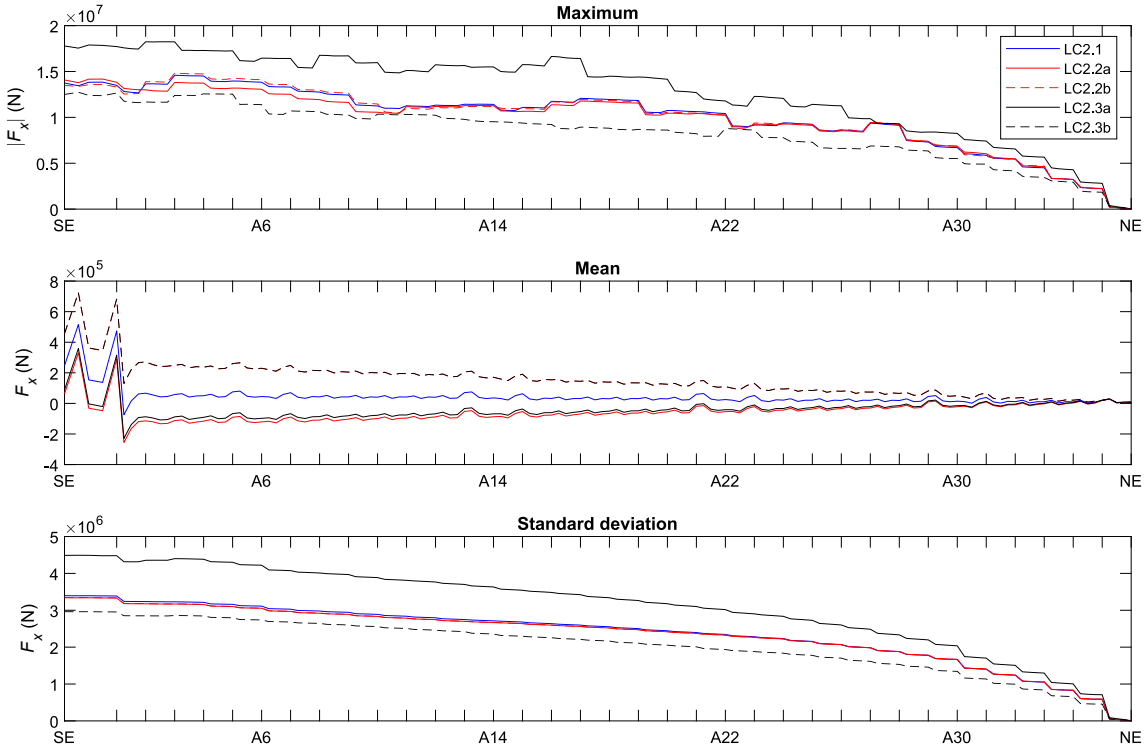

Fig. 21. Statistical values of axial force for 100-year load cases.

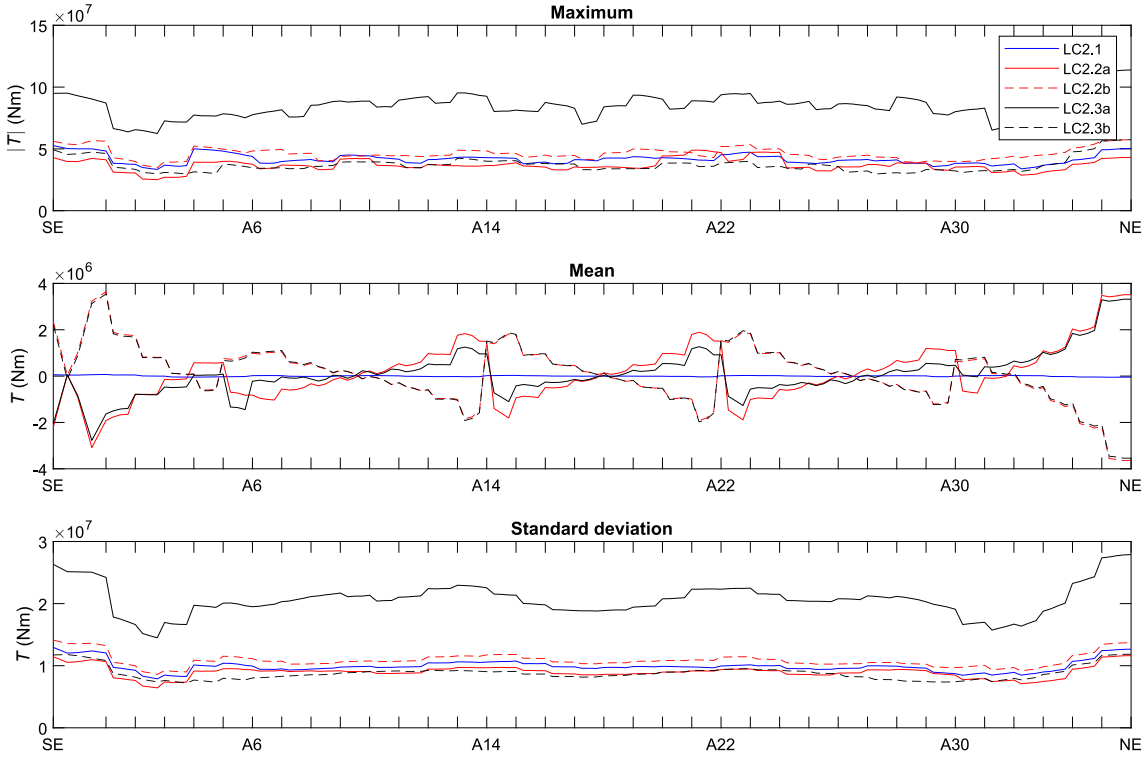

Fig. 22. Statistical values of torsion for 100-year load cases.

Declaration of Competing Interest

The authors declare that they have no known competing financial interests or personal relationships that could have appeared to influence the work reported in this paper.

Acknowledgments

This work was supported by the Research Council of Norway through the project 268403/O80 Design and Verification of Large Floating Coastal Structures – Environmental description, structural loads,

responses and mooring system. The authors are grateful to the Norwegian Public Roads Administration for the permission to use and publish the experimental data.

References

[1] Xu Y, Øiseth O, Moan T. Time domain simulations of wind- and wave-induced load effects on a three-span suspension bridge with two floating pylons. Mar struct 2018;58:434–52.

[2] Sha Y, Amdahl J, Aalberg A, Yu Z. Numerical investigations of the dynamic response of a floating bridge under environmental loads. Ships Offshore Struct 2018;13:113–26.

[3] Cheng Z, Gao Z, Moan T. Hydrodynamic load modeling and analysis of a floating bridge in homogeneous wave conditions. Mar Struct 2018;59:122–41.

[4] Dai J, Leira BJ, Moan T, Kvittem MI. Inhomogeneous wave load effects on a long, straight and side-anchored floating pontoon bridge. Mar Struct 2020;72:102763. https://doi.org/10.1016/j.marstruc.2020.102763.

[5] Deng S, Ren H, Xu Y, Fu S, Moan T, Gao Z. Experimental study on the drag forces ona twin-tube submerged floating tunnel segment model in current. Appl Ocean Res 2020;104:102326. https://doi.org/10.1016/j.apor.2020.102326.

[6] Statens vegvesen. Costal highway route E39 project. Teknologidagene, Trondheim, 22 September, 2015.

[7] Cheng Z, Gao Z, Moan T. Numerical modeling and dynamic analysis of a floating bridge subjected to wind, wave and current loads. J Offshore Mech Arct Eng 2019; 145(1):05018008.

[8] Multiconsult. SBJ-31-C3-MUL-22-RE-100-0 – Analysis and design (Base Case). Multiconsult AS, Oslo, Norway; 2017.

[9] DNV GL. SBJ-31-C3-DNV-62-RE-018-0 Bjørnafjorden side anchored floating bridge - independent global analyses. DNV GL, Oslo, Norway; 2018.

[10] Huang NE, Chen DT, Tung C-C. Interactions between steady non-uniform currents and gavity waves with applications for current measurements. J Phys Oceanogr 1972;2:420–31.

[11] Hedges TS, Anastasiou K, Gabriel D. Interaction of random waves and currents. J Waterw Port Coastal Ocean Eng 1985;111(2):275–88.

[12] Ismail NM. Wave-current models for design of marine structures. J Waterw Port Coastal Ocean Eng 1984;110(4):432–47.

[13] Liu Z, Teng B, Ning D, Gou Y. Wave-current interactions with three-dimensional floating bodies. Journal of Hydrodynamics, Ser. B 2010;22(2):229–40.

[14] Hermundstad EM, Hoff JR, Stansberg CT, Baarholm R. Effects of wave-current interaction on floating bodies. Proceedings of the 35th International Conference on Ocean, Offshore and Arctic Engineering, Busan, South Korea, 19-24 June, 2016.

[15] Chen L, Basu B. Wave-current interaction effects on structural responses of floating offshore wind turbines. Wind Energy 2019;22(2):327–39.

[16] Wei C, Zhou D, Ou J. Wave and wave-current actions on a bridge tower: An experimental study. Adv Struct Eng 2019;22(6):1467–78.

[17] Viuff T, Xiang Xu, Øiseth O, Leira BJ. Model uncertainty assessment for wave- and current-induced global response of a curved floating pontoon bridge. Appl Ocean Res 2020;105:102368. https://doi.org/10.1016/j.apor.2020.102368.

[18] Statens vegvesen. SJB-01-C4-SVV-01-BA-001 MetOcean Design basis. Statens vegvesen, Oslo, Norway; 2018.

[19] Statens vegvesen. SBJ-32-C3-SVV-BA-002 Design Basis Bjørnafjorden Rev E. Statens vegvesen, Oslo, Norway; 2018.

[20] Morison JR, O'Brien M, Johnson J, Schaaf S. The forces exerted by surface waves on piles. J Petrol Technol 1950;2(05):149–54.

[21] Newman JN. Marine Hydrodynamics. Cambridge, MA: The MIT Press; 2017.

[22] Faltinsen OM. Sea Loads on Ships and Offshore Structures. Cambridge, UK: Cambridge University Press; 1990.

[23] DNV GL. Offshore Standard DNVGL-OS-E301: Position mooring. DNV GL, Oslo, Norway; 2018.

[24] Newman JN. The quest for a three-dimensional theory of ship-wave interactions. Philos Trans Roy Soc A 1991;334:213–27.

[25] Journée JMJ, Massie WW. Offshore Hydromechanics. 2nd edition. the Netherlands: Delft University of Technology; 2008.

[26] Cummins WE. The impulse response function and ship motions. Report No. DTMB-1661, Washington DC, USA; 1962.

[27] DNV GL. SESAM release note: SIMA V4.1.0. DNV GL, Oslo. Norway; 2021.

[28] SINTEF Ocean. SIMO 4.18.1 theory manual. SINTEF Ocean, Trondheim, Norway; 2020.

[29] SINTEF Ocean. RIFLEX 4.18.1 theory manual. SINTEF Ocean, Trondheim, Norway; 2020.

[30] WAMIT. WAMIT User Manual version 7.3. WAMIT, Chestnut Hill, USA; 2019.

[31] Det Norske Veritas. SEASAM User Manual – Wadam. Det Norske Veritas, Norway; 2014.

[32] SINTEF Ocean. Veres3D User Manual. SINTEF Ocean, Trondheim, Norway; 2020.

[33] Cheng Z, Svangstu E, Gao Z, Moan T. Field measurements of inhomogeneous wave conditions in Bjørnafjorden. J Waterw Port Coastal Ocean Eng 2019;145(1): 05018008.

[34] Havforskningsinstituttet. Fisken og Havet. 2011(2). NorKyst-800 Report No. 1. User Manual and technical descriptions. Havforskningsinstituttet, Norway; 2018.

[35] Cheng Z, Gao Z, Moan T. Wave load effect analysis of a floating bridge in a fjord considering inhomogeneous wave conditions. Eng Struct 2018;163:197–214.

[36] Dai J, Leira BJ, Moan T, Alsos HS. Effect of wave inhomogeneity on fatigue damage of mooring lines of a side-anchored floating bridge. Ocean Eng 2021;219:108304. https://doi.org/10.1016/j.oceaneng.2020.108304.

[37] Hasselmann K, Barnett TP, Bouws E, Carlson H, Cartwright DE, Enke K, et al. Measurements of wind-wave growth and swell decay during the Joint North Sea Wave Project (JONSWAP). Ergän Deuts Hydrographischen Z Reihe 1973;A12(8): 1–95.

[38] Statens vegvesen. Modellforsøk med Flytebru: Kontinuerlig Pontongbru. Report no. MT40 F89-0252. Statens vegvesen, Oslo, Norway;1989.

[39] Lwin M. Floating bridges. Bridge Engineering Handbook. Boca Raton, USA: CRC Press; 2000.

[40] Wan L, Jiang D, Dai J. Numerical modelling and dynamic response analysis of curved floating bridges with a small rise-span ratio. J Mar Sci Engi 2020;8(6):467. https://doi.org/10.3390/jmse8060467.